Rendiconti Lincei. Scienze Fisiche e Naturali
https://doi.org/10.1007/s12210-024-01298-x

Investigating stone materials from some European cultural heritage sites for predicting future decay

Chiara Coletti[1] · Fabrizio Antonelli[2] · Luigi Germinario[1] · Lara Maritan[1] · Rebecca Piovesan[2] · Elena Tesser[2] · Claudio Mazzoli[1]

Received: 3 November 2024 / Accepted: 21 December 2024

Abstract

The preservation of Europe's stone-built heritage is crucial for safeguarding our cultural legacy. This study investigates twelve distinct stones used in historical monuments across Italy, Spain, Greece, and Norway, including marbles (Carrara and Macael), limestones (Botticino, Red Verona, Costozza, Istrian, Sfouggaria, Santa Pudia), a carbonate-dominated sandstone (Lartios), volcanic rocks (Euganean trachyte and Tønsberg latite), and an intrusive igneous rock (Tønsbergite). Through comprehensive analysis of mineralogical composition, porosity, water interactions, and accelerated ageing tests, this research establishes a framework for assessing these materials susceptibility to decay mechanisms. The results demonstrate significant variability in durability and decay response among the stone types, primarily determined by pore abundance and distribution. This study enhances the understanding of stone materials behaviour under stressed conditions, offering valuable insights for mitigating future decay processes and protecting European cultural heritage. The stones examined were chosen for their significant presence at the four pilot sites of the European Hyperion project: Venice (Italy), Granada (Spain), Rhodes (Greece), and Tønsberg (Norway).

This research paper belongs to the Topical Collection "LAMA 1994-2024: Archaeometric and Conservation Studies of the Cultural Heritage in the Mediterranean Basin", celebrating thirty years of activity of the Laboratory for Analysing Materials of Ancient origin (LAMA) at the Iuav University of Venice, Italy. Guest Editor F. Antonelli.

✉ Claudio Mazzoli
claudio.mazzoli@unipd.it

[1] Department of Geosciences, University of Padova, Via Gradenigo 6, 35131 Padua, Italy

[2] LAMA-Laboratory for the Analysis of Ancient Materials, University Iuav of Venice, Calle Della Laca, San Polo, 2468, 30125 Venice, Italy

Published online: 22 January 2025

Graphic abstract

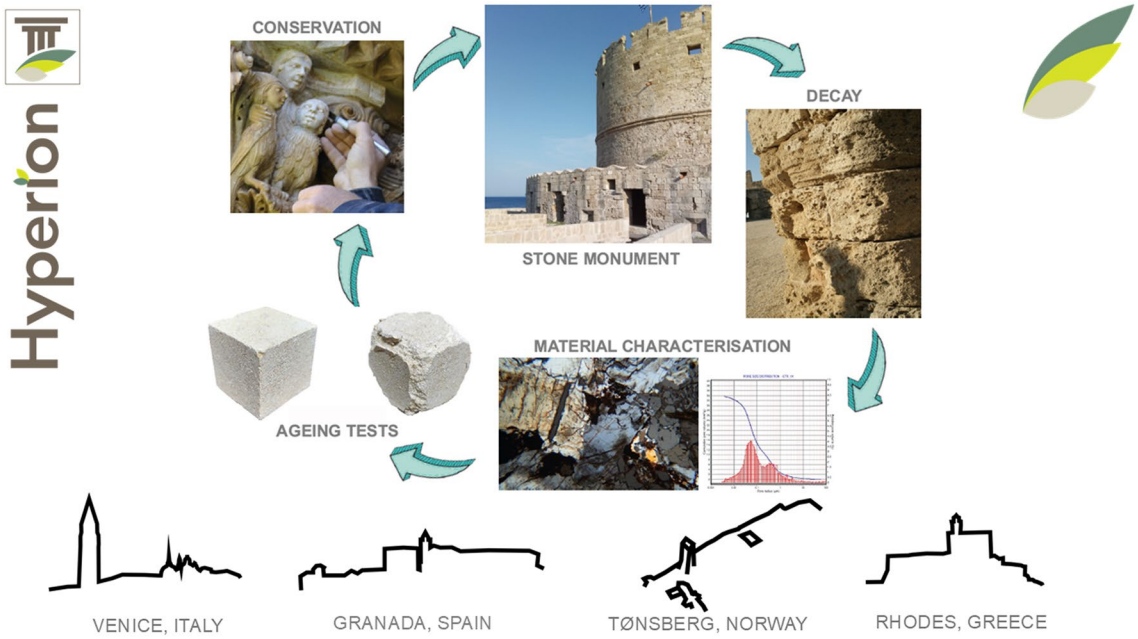

Keywords Building stones · Technical properties · Pore-size distribution · Hygrothermal properties · Ageing tests

1 Introduction

The deterioration of historical stone-built heritage presents a significant conservation challenge, requiring a comprehensive approach that considers building materials, preventive measures, restoration strategies, and adaptation methodologies. Understanding the decay processes affecting stone heritage and predicting future risks to its preservation are closely linked to the properties of the materials and their responses to environmental stresses. In light of climate change, researchers have increasingly focussed on quantifying the degradation of historical monuments (Bonazza et al. 2009a, b; Salvini et al. 2022; Hernández-Montes et al. 2022; Germinario et al. 2023). Despite these efforts, the urgency of the climate crisis and the complexity of developing universally applicable predictive models for stone decay make continued investigation essential (Coletti 2024; Zaccariello et al. 2024). This study presents an analysis of various stone materials used in historic European buildings, aiming to establish correlations between their physicochemical and mineralogical properties and observed decay and vulnerability patterns. Furthermore, it provides insights into ageing patterns and kinetics, which differ based on the intrinsic characteristics of the materials.

The selected materials include igneous, sedimentary and metamorphic stones from Italy, Greece, Spain, Norway and Croatia, known for their historically significant and commercial value. Most of these rocks are carbonate in nature, but some silicate stones are also included.

The stones investigated were chosen from the best-known and most widely used in four European historic sites selected as pilot locations by the European Hyperion project, under which this research was conducted. The cities are Venice (Italy), Rhodes (Greece), Granada (Spain) and Tønsberg (Norway), representing different climate and environmental conditions.

Venice has a humid subtropical climate, characterised by hot, muggy summers and cold, humid winters, with an annual average precipitation of approximately 800 mm, a mean summer maximum temperature of 28.3 °C, and a mean winter minimum temperature of 2.7 °C, with rare freezing events. Venice is situated in a lagoon environment and is increasingly exposed to high tides due to a combination of subsidence, sea level rise, and intensification of extreme weather events (Lionello et al. 2021). In 2019, the city experienced a tide as high as 187 cm, resulting in the worst flooding since the 194 cm high tide of 1966. Rising sea level and high tide events increasingly expose brick walls of buildings to water capillary rise and salt crystallisation. Moreover, monuments in Venice exhibit other typical decay forms, including black crusts, biological growth, and fouling in the intertidal zone (Piovesan et al. 2023a, 2024).

Rhodes has a typical Mediterranean climate, with hot, sunny summers and mild, rainy winters. Average annual

precipitation is approximately 650 mm, mainly occurring between November and February, with average temperatures ranging between 29.2 °C and 11.6 °C. Due to the proximity to the sea, freezing temperatures in Rhodes are rare. The primary deterioration mechanisms are linked to marine aerosols, which expose stone to salt crystallisation (Stefanis et al. 2009; Apostolopoulou et al. 2019).

Granada is located on the eastern edge of a basin at the foothills of the Sierra Nevada, at an elevation of approximately 700 m and 60 km inland. The area has a Mediterranean climate influenced by Atlantic and continental disturbance, resulting in dry, sunny, and relatively short summers and long, mostly cloudy, and humid winters. Average annual precipitation is approximately 500 mm, occurring between October and May, with average temperatures ranging from 33 °C to 2 °C. The region experiences about 20–25 frost days per year and diurnal temperature variations of up to 30 °C, which lead to significant fluctuations in relative humidity (Arizzi et al. 2012). In this environment, and given that Granada is one of the most polluted cities in Spain, freeze–thaw cycles and salt crystallisation, particularly sulphates and magnesium salts, are the primary cause of deterioration (Ruiz-Agudo et al. 2011; Kontozova-Deutscha et al. 2011).

Due to its higher latitude, Tønsberg experience significantly differ climate conditions compared to the other localities. It has a humid continental climate, with short, warm summers reaching maximum temperatures of about 20 °C in July and August, and long, cold winters with minimum temperatures of approximately −5 °C from December to February. Average annual precipitation exceeds 1000 mm, and is evenly distributed throughout the year, with peak frequencies from September to November. Under these environmental conditions, frost action, interactions with rainwater or snow, and biological growth are the main threats to heritage buildings.

The vulnerability assessment of stone building materials is closely related to the specific environmental conditions and the petrophysical properties of the stones.

For this study, the selected stones include: six limestones (Botticino stone, Red Verona stone, and Costozza stone from Italy; Istrian stone from Croatia; Sfouggaria stone from Rhodes, Greece; Santa Pudia stone from Spain), one carbonate-dominated sandstone (Lartios stone from Rhodes, Greece), two white marbles (Carrara marble from Italy; Macael marble from Spain), two volcanic rocks (Euganean trachyte from Italy; Tønsberg latite from Norway), and one intrusive igneous rock (Tønsbergite from Norway).

There is ample evidence in the literature regarding the use of these stones in cultural heritage broadly (Alcalde et al. 1992; Antonelli et al. 2004; Benchiarin 2007; Antonelli and Lazzarini 2012, 2015; Germinario et al. 2018a, b; Sciarretta et al. 2018; Renzulli et al. 2019; Taelman et al. 2019; Stamati et al. 2022; Bernardini et al. 2023; Salvini et al. 2023a) or more specifically in the mentioned cities (Lazzarini 2012; Luque et al. 2010; Piovesan et al. 2023a). For instance, Piovesan et al. (2023a) identified that the Clock Tower in Venice, a case study selected in the Hyperion project, was clad with a combination of Istrian stone, Red Verona stone, and Carrara marble, among others. Numerous studies also discuss their state of decay and deterioration or their response to different cleaning or conservation treatments (Lazzarini et al. 2012; Salvi et al. 2012; Vázquez et al. 2013; Antonelli et al. 2016; Tesser et al. 2014, 2017, 2018; Tesser and Antonelli 2018; Gheno et al. 2018; Galanaki et al. 2022; Salvini et al. 2023a, b; Piovesan et al. 2024; Zaccariello et al. 2024). However, some stones, such as those here considered from Norway and Rhodes, have not been extensively investigated in this context. Therefore, this work offers the first concrete data for the characterization of these lithologies, with reference to the processes mentioned.

These materials were studied in the laboratory using a petrographic and physical–mechanical approach, encompassing a series of analyses aimed at determining a range of properties related to material texture, colour, density, porosity, water, vapour and thermal behaviour, strength, deformability and resistance to artificially accelerated weathering through salt crystallisation and freeze–thaw tests.

The various properties of the materials investigated are presented and interpreted here to highlight correlations between differences in material damages and their compositional and textural properties. This study aims to provide valuable information on the quality, durability, and suitability of each material, offering insights useful for understanding past deterioration and predicting future risks to cultural heritage assets made of the same (or similar) materials.

2 Materials

2.1 Botticino stone

Botticino stone is an early Jurassic, partially dolomitised micritic limestone belonging to the Corna Formation (Table 1). This formation consists of various facies typical of a subtidal platform, such as mudstone, floatstone, and wackestone, with fossil assemblages including oncolites, dasycladacean algae, red algae, and other bioclasts, often heavily obliterated by intense dolomitization (Schirolli 1997; Di Battistini et al. 2005; Borghi et al. 2015; Masetti et al. 2017). Quarries are located in the Botticino, Rezzato, and Mazzano areas (Brescia, northern Italy), primarily concentrated in the upper stratigraphic units. These units show an increase in pelagic and deep-sea facies, represented by cream-colored and reddish mudstones and wackestones

Table 1 Summary of the main petrographic classifications and geological information of the stones examined in this study, along with examples of notable monuments in which they were used (details provided in the text)

Name	Quarry location	Rock type	Geological formation	Age	Relevant monuments
Botticino stone	Rezzato, Mazzano (Brescia, Italy)	Floatstone/Crystalline carbonate	Corna Formation	Early Jurassic	Brescia: Vespasian Temple, Theatre, Forum, Baths (Roman), Santa Maria dei Miracoli, Palazzo della Loggia, New Cathedral; Osaka: Chamber of Commerce; Jeddah: Red Sea Hospital; Boston: One International Place
Red Verona stone	Venetian Prealps (NE Italy)	Mudstone/Floatstone	Rosso Ammonitico Veronese Formation	Middle-late Jurassic	Verona: "Arena", Ponte Pietra; Cathedrals of Bologna, Parma, Cremona; Bergamo: Santa Maria Maggiore; Venice: Ducal Palace, St. Mark's Basilica
Costozza stone	Berici Hills (Vicenza, Italy)	Grainstone/Rudstone	Castelgomberto Limestone Formation	Oligocene	Palladian Villas of Veneto; Modena: Cathedral, the Ghirlandina; Padova: statues in Prato della Valle square
Istrian stone	Vrsar, Rovinj (Istria, Croatia)	Mudstone	Kirmenjak Unit	Late Tithonian	Venice: Rialto Bridge, Bridge of Sights, Ducal Palace, Palladio churches; Poreč: Euphrasian Basilica; Ravenna: Mausoleum of Theodoric, Dante Alighieri's tomb, S. Agata
Sfouggaria stone	Eastern coast of Rhodes (Greece)	Grainstone/Rudstone	Rhodes Formation	Pliocene–Pleistocene	City of Rhodes
Lartios stone	Lardos, Lindos (Rhodes, Greece)	Carbonate-dominated sandstone	Kattavia Flysch	Lower Oligocene	Rhodes: Theon Panton sanctuary, Lindos and Kymissala Acropolises, base for the Nike of Samothrace
Santa Pudia stone	Escuzar (Andalusia, Spain)	Grainstone/Rudstone	Granada basin	Tortonian	Granada: Cathedral, Royal Hospital, Palace of Carlos V, Royal Chapel, San Jerónimo Monastery; Córdoba: Mosque; Seville: Cinco Llagas Hospital
Carrara marble	Apuan Alps (Tuscany, Italy)	Marble	Tuscan Nappe	Early Jurassic,	Rome: Pantheon, Trajan's and Marcus Aurelius' Columns; statues by Michelangelo, Donatello, Jacopo della Quercia, Bernini, Canova, Rodin, and others; Florence: Cathedral, Baptistery, Giotto's Bell Tower

Table 1 (continued)

Name	Quarry location	Rock type	Geological formation	Age	Relevant monuments
Macael marble	Macael (Almería, Spain)	Marble	Nevado-Filábride Complex	Palaeozoic?	Roman towns of Itálica (Seville) and Sagunto (Valencia); Córdoba: Madinat al-Zahra palace-city, Mosque; Almería: Alcazaba; Granada: Court of the Lions, Hall of the Two Sisters (Alhambra)
Euganean trachyte	Euganean Hills (Veneto, Italy)	Trachyte	Venetian Volcanic Province	Early Oligocene	Roman millstones, mortars, milestones, stèles, tombstones, sarcophagi, paving stones, flagstones, structural elements for roads, bridges, aqueducts, harbours; Middle Ages and Renaissance architectonic elements
Tønsberg latite	Tønsberg (Oslo, Norway)	Latite	Oslo graben	Late Carboniferous-early Permian	Tønsberg: Slottsfjell tower
Tønsbergite	Tønsberg (Oslo, Norway)	Qtz-bearing larvikite (variety of syenite)	Oslo graben	Late Carboniferous-early Permian	Oslo: Freemasons' hall

containing peloids, crinoids, echinoids, and sponge spicules, with cherts, indicating the progressive drowning of the carbonate platform (Schirolli 2007). The variety commercially known as *Botticino Classico* Marble is extracted from an open-air quarry on the south-western side of Mt. Fratta, in the territory of Botticino. This stone has been used in Brescia since Roman times, notably in the Temple of Vespasian, the Theatre, the Forum, and the Baths. Later, it was employed in several buildings in the same city, including the Church of Santa Maria dei Miracoli, the Palazzo della Loggia, and the New Cathedral. At the end of the nineteenth century, *Botticino Classico* gained wider recognition beyond the Brescia province, largely due to its use in the construction of the Vittoriano in Rome, commemorating Vittorio Emanuele II. Since then, the use of *Botticino Classico* has proliferated throughout Italy (e.g. Victory Monument in Bolzano, Palace of the Commercial Italian Bank in Milan) and worldwide (e.g. some architectonic elements of the White House in Washington, of the Grand Central Terminal and of the basement of the Statue of Liberty in New York, the Chamber of Commerce in Osaka, the façade of the Red Sea Hospital in Jeddah, and the One International Place in Boston), both as cladding and as a structural element (Clerici and Meda 2005; Salvini et al. 2023a).

2.2 Rosso di Verona / Red Verona stone

Rosso di Verona, Red Verona stone, or Red Verona Marble, is the commercial name for the nodular, ammonite-bearing limestone from the *Rosso Ammonitico Veronese* Formation, a late Bajocian to Thitonian condensed sedimentary succession deposited on the distal Trento Plateau (Table 1). Petrographically, it includes mudstone and floatstone with varied colouring that ranges from red-brown or red–orange to yellow and white, depending on the concentration of iron oxides and clay minerals. The biogenic components include planktonic and benthic foraminifera, radiolarians, calcispheres, and planktonic bivalves (Albertini 1991; Préat et al. 2006). This formation has been extensively exploited in the Venetian Prealps since Roman times and has been widely used as dimension stone, particularly in northeastern Italy. The Roman amphitheatre "Arena" and the Ponte Pietra (Stone Bridge) in Verona are almost entirely made of this stone, as well as several elements of the Roman theatre. The cathedrals of Bologna, Parma, and Cremona, as well as the lions located at the entrance of the Basilica of Santa Maria Maggiore in Bergamo, are just a few examples of the numerous historical uses of Red Verona stone. In Venice, many elements of the Ducal Palace and St. Mark's Basilica, along with numerous palaces, square pavements, and well curbs, are made from this stone, often in combination with white Istrian stone to create ornamental effects. Due to its historical significance, *Rosso di Verona* stone has recently

been proposed for designation as an IUGS Global Heritage Stone Resource (GHSR) (Primavori 2020).

2.3 Costozza stone

Costozza stone is a light ivory variety of Vicenza stone, an ornamental stone extracted from the Berici Hills near Vicenza (north-eastern Italy) (Table 1). Lithostratigraphically, Vicenza stone represents a specific lithofacies within the lower Oligocene Castelgomberto Formation, characterised by compact 2– 10 m thick horizons of grainstone, floatstone and rudstone with miliolids, red algae, encrusting foraminifera, and large foraminifera such as *Amphistegina*, *Operculina*, *Nummulites* and other rotaliids (Nebelsick et al. 2005, 2013). The matrix is scarce or absent, and the bioclasts are cemented by an isopachous calcite cement, resulting in high porosity. This high porosity contributes to its high softness, which makes Vicenza stone highly workable, earning it the name Pietra Tenera (Soft Stone) of Vicenza. Vicenza stone has been quarries from over one hundred underground sites since the Roman times for statues, headstones, and architectural elements. Its most iconic use, however, is in the construction of public palaces, private villas, and churches designed by architects Andrea Palladio and Vincenzo Scamozzi in Vicenza and the surrounding territories, all of which are part of the UNESCO World Heritage Site "City of Vicenza and the Palladian Villas of the Veneto". Additionally, the Cathedral of Modena and the Ghirlandina, part of the UNESCO World Heritage Site "Cathedral, Torre Civica and Piazza Grande, Modena", and the 78 statues in Prato della Valle square in Padova are also crafted from Vicenza Stone (Cornale and Rosanò 1994; Braga 2004). For this reason, Vicenza Stone, like Red Verona stone, has also been proposed for designation as an IUGS Global Heritage Stone Resource (GHSR) (Milizia et al. 2022).

2.4 Istrian stone

Istria extends over a wide late Jurassic to Eocene carbonate platform, with a long-standing tradition of stone exploitation, evidenced by thousands of quarries in the region (Table 1). The highest quality material is represented by a 65 m thick layer of compact fine-grained stylolitic limestone from the late Tithonian Kirmenjak unit (Durn et al. 2003). This white to light grey limestone is characterised by low porosity, conchoidal fracture, and mechanical properties comparable to marble (Geometrante et al. 2000). The most important quarries for the Venetian architecture are located near Vrsar (Orsera) and Rovinj (Lazzarini 2012). While the use of the Istrian stone dates back to Roman times, it was not widely exported, with rare examples found in Aquileia. Its application in Venice, however, was already established in the thirteenth century, primarily for statuary. In 1307, the Venetian Senate decreed that Istrian stone should be the only stone building material used for Venetian structures throughout all Venetian territories. Dunda and Kujundžić (2004) estimated that 80% of the stones used in Venice from that point onward came from Istria. The considerably low porosity of the stone (usually significantly below 1%), made it ideal for foundational use. Continuous courses of Istrian stone, known as "cadene", were placed above the average high tide level to protect brick walls from capillary water rise (Foraboschi 2017). Istrian stone was also extensively used for cladding. In Venice (part of the UNESCO World Heritage Site "Venice and its Lagoon"), many buildings are entirely clad in this stone, including the Rialto Bridge, the Bridge of Sights, and the lower and second external galleries, along with the courtyard of the Ducal Palace. The upper walls of this building feature a two-tone geometric pattern created by combining Istrian stone and Red Verona stone. Andrea Palladio, who primarily employed Vicenza stone in many of his works, opted for Istrian stone for architectural continuity in his Venetian works in the sixteenth century, such as the façades for the Basilica of San Pietro di Castello, of the churches of San Francesco della Vigna, San Giorgio Maggiore, and Il Redentore. Beyond Venice, Istrian stone was also used in Thessaloniki (Greece), Dubrovnik (Croatia), the Euphrasian Basilica in Poreč (Croatia), and the Mausoleum of Theodoric, the Lombardesque structures of Dante Alighieri's tomb and the portal of the church of S. Agata in Ravenna, just to cite a few UNESCO World Heritage Sites (Borghi et al. 2015; Lazzarini 2012; Salvini et al. 2023a).

2.5 Sfouggaria stone

Along the eastern coast of Rhodes, Pliocene–Pleistocene temperate littoral and marine sediments are well-documented (Table 1). These sediments were deposited in tectonically driven micro-grabens, characterised by a complex pattern of heteropic facies that reflect numerous transgressive and regressive cycles. The deposits include siliciclastic and bioclastic sediments, as well as terrigenous pelagic muds and deep-sea carbonates. Stratigraphically, they are formalised into four formations: the Pliocene Cape Vigli Formation, composed of highly fossiliferous sandy to silty mudstones containing a diverse mollusc assemblage, including *Pinna nobilis*, *Megaxinus ellipticus*, and *Persististrombus coronatus*; the early Pleistocene Kritika Formation, composed primarily of siliciclastic deposits; the Rhodes Formation, which records a complete major Pliocene–Pleistocene transgressive–regressive cycle with marine deposits; and the Lindos Acropolis Formation, which unconformably overlies the Rhodes Formation and contains conglomeratic

facies with pebbles and boulders of the Rhodes Formation and basement clasts. These formations are further subdivided into facies groups. Biocalcarenites (grainstone, rudstone and floatstone) from the Rhodes Formation belong to the Cape Arkhangelos Calcarenite (Hanken et al. 1996; Hansen 1999; Titschack et al. 2005; Lekkas et al. 2007; Schneider et al. 2023). This calcarenite has been extensively exploited since antiquity, with numerous ancient quarries visible along the coast from Rhodes to Lindos. It has served as the primary building material for the city of Rhodes (a UNESCO World Heritage Site) since its foundation in 408 BCE, continuing through the end of the Turkish Empire. In the Middle Age, the Byzantine period, and the following period of the knights, material derived from the spoliation of ancient structures, the creation and deepening of the moat, and the numerous quarries along the northeastern coast. This calcarenite was used for the construction of fortifications and buildings, as well as for the extensive restauration and reconstruction during the Italian occupancy of the fascist regime period (Kollias 1989). The most prominent ancient quarries are located in the Stegna area, from where the Sfouggaria limestone sample for this study was obtained. Apostolopoulou et al. (2019) characterised samples from the same quarry in their study on the restoration project of the Apollo Pythios Temple, determining the petrographic, mineralogical, chemical, microstructural, hygric, mechanical and aesthetic properties of this calcarenite. Moropoulou et al. (2000) found a significant correlation between the weathering index of biocalcarenites from various Mediterranean localities, including the stone used in Rhodes, and the sea-salt crystallisation pressure, calculated using a probabilistic thermodynamic approach on total porosity and pore-size distribution. Additionally, Galanaki et al. (2022) conducted accelerated ageing tests using sodium chloride solution on the same stone type to investigate its durability against salt crystallization.

2.6 Lartios stone

Lartios stone, or *lithos lartios*, is a grey-blue carbonate stone characteristic of Rhodes, historically quarried near the village of Lartos (modern-day Lardos, in the municipality of Lindos) primarily for local use (Papavassiliou et al. 2020). The quarrying sites around Lardos are all located in the lower Oligocene sequences of the Kattavia Flysch, with weakly metamorphosed terms belonging to the Kalathos Member, spatially restricted to the region west of Lindos (Mutti et al. 1970) (Table 1). In the Lardos area and immediately to the west in the Mt. Horti area, grey limestones alternate with lithic turbiditic sandstones and sandy nummulitic detrital limestones (Mutti et al. 1970).

In antiquity, Lartios stone was used for various purposes, including a Hellenistic road in the city of Rhodes paved with this stone (Archibald 2013). It also served for sculpturing portrait statues for funerary and honorific purposes during the Hellenistic period, along with marble (Bairami 2017). Artefacts such as pedestals, altars, and decorative mouldings crafted from Lartios stone have been found at the Lindos Acropolis and in the city of Rhodes dating back to the Classical and Hellenistic periods (Bruno et al. 2015). The Late Hellenistic-Roman altar of the *Theon Panton* sanctuary in Rhodes has foundation and the euthynteria elements made of large blocks of this stone, exhibiting finely chiseldrafted margins at the facing surface (Bairami 2023). In the Hellenistic temple at Kymissala Acropolis (3rd–second century BCE), Lartios stone was also used as dimension stone, though sourced from quarries at the nearby *Marmarounia* hill instead of Lardos (Stamati et al. 2022). Three main quarrying areas for Lartios stone have been identified based on ancient tool marks and abandoned semi-finished pieces: near Lardos, at Kymissala, and at Lyros, north of Kymissala. These sites exhibit slight variations in texture and colour. Maniatis et al. (2015) distinguished these quarrying districts through textural analysis, EPR spectroscopy, and stable isotope analysis. Documented exports of Lartios stone are rare, with only two known cases: an inscribed stele found on Karpathos and the ship bow base for the Nike of Samothrace (Maniatis et al. 2012; Bruno et al. 2015).

2.7 Santa Pudia stone

Santa Pudia stone is a white to yellow, porous limestone that is relatively soft and quarried from the Cortijo de Santa Pudia zone in Escuzar, located about 30 km southwest of Granada (Andalusia, Spain). It consists of Tortonian temperate-water carbonates that were deposited within the intramontane Granada Basin, formed during the late extensional phase of the Betic Cordillera orogeny (Corbí et al. 2012; López-Quirós et al. 2016) (Table 1). Historically, Santa Pudia stone has been extensively used in Granada iconic architecture, such as the Cathedral, the Royal Hospital, the Palace of Carlos V, the Royal Chapel and the San Jerónimo Monastery. It has also been employed in the restoration projects for the Mosque of Córdoba and the Cinco Llagas Hospital in Seville.

Owing to its historical significance as a building material, the stone has been the subject of numerous studies addressing its petrographic and physical characteristics (Molina et al. 2011, 2013), mechanical properties (Rodriguez-Navarro 1994), and creep behaviour (Gil-Martín et al. 2023). Research has also focussed on the influence of pore system and clay content on durability (Molina et al. 2011, 2013), as well as the susceptibility of Santa Pudia stone to pollution and salt crystallization. Additionally, the distinctive deterioration patterns observed on monuments constructed from this stone have been documented, describing the specific visual and physical manifestations of weathering (Alcalde

et al. 1992; Rodriguez-Navarro 1994; Rodriguez-Navarro and Sebastian 1996; de Jong van Coevorden et al. 2012; Ruiz-Agudo et al. 2024). Further studies have evaluated the effectiveness of various treatments aimed at enhancing the stone durability (Cultrone et al. 2007; Luque et al. 2008; Molina et al. 2011, 2013; Vázquez et al. 2013) and the impact of surface finishing on its deterioration rate (Molina et al. 2020). Jalón et al. (2020) proposed a comprehensive degradation model for Santa Pudia stone, further contributing to the understanding of its long-term performance in historical architecture.

2.8 Carrara marble

Carrara marble is one of the world's most renowned stones, prised for its quality and historical significance. Its extraction dates back to pre-Roman times from the Apuan Alps (northwestern Tuscany, Italy). The marble originates form thick Mesozoic carbonate sequences of the Tuscan Nappe, which underwent low-grade metamorphism during the Eocene-early Miocene continental collision between Europe (Sardinia/Corsica) and Adria plates (Molli et al. 2000) (Table 1). This marble has been extensively used since pre-Roman times (Antonelli and Lazzarini 2013), serving as a preferred material for sculptures and architecture during the Roman period (Antonelli and Lazzarini 2015), and the Renaissance (Berto et al. 2012). Numerous globally significant heritage monuments utilise Carrara marble, including the Pantheon, Trajan's and Marcus Aurelius' Columns, Michelangelo's Pietà in Rome, and Michelangelo's David (and other his sculptural masterpieces) in Florence, as well as the Cathedrals of Massa and Carrara, and the Ducal Palace of Massa. In Florence, the Cathedral, the Baptistery, and the Giotto's Bell Tower prominently use Carrara marble alongside other coloured stones. The marble popularity continued over the centuries, with artists like Donatello, Jacopo della Quercia, Bernini, Canova, and Rodin, crafting iconic works from it. In modern times, prestigious landmarks such as the Marble Arch in London (1827), Harvard Medical School in Boston (1906), the episcopal throne in the Cathedral of Manila (The Philippines) (1958), the Finland Hall in Helsinki (Finland) (1971), the Opera House in Oslo (Norway) (2007), the Sheikh Zayed Grand Mosque in Abu Dhabi (2007), the Prem Mandir Hindu Temple in Vrindavan (India) (2012), have all incorporated Carrara marble. The stone varieties range from the classical White Carrara marble, an ivory white fine- to medium-grained homogeneous calcitic marble, to versions with spotty, brecciated, or veined patterns. These different types are currently quarried at an annual rate of 1.5 million tonnes (Primavori 2015; Salvini et al. 2023a). Acknowledging its cultural significance, Carrara marble was designated as an IUGS Heritage Stone in 2017 by the Subcommission on Heritage Stones of the International Commission on Geoheritage.

2.9 Macael marble

Like Carrara marble, Macael marble was also designated as an IUGS Heritage Stone in 2019 due to its cultural significance. It is a coarse-grained, purely calcitic white marble, with some varieties also containing micas, quartz, and opaque minerals, which create grey banding. Named after the town of Macael (Almería, Spain), it has been continuously quarried since Neolithic times, including during the Phoenician, Roman, Muslim, and Renaissance periods. During the Roman Empire White Macael marble was use for headstones, statues, inscriptions, and architectural elements in Roman cities such as Itálica (Seville) and Sagunto (Valencia). Under the Muslim rule in the Middle Ages, Macael marble adorned many monumental structures, including the façades, capitals, baths, and columns of the Madinat al-Zahra palace-city and the Mosque-Cathedral of Córdoba (both UNESCO World Heritage Sites), as well as the Alcazaba in Almería, and the iconic Court of the Lions and the Hall of the Two Sisters in the Alhambra (UNESCO World Heritage Site) in Granada (Bello et al. 1992; Navarro et al. 2019). Geologically, Macael marble, along with associated schists, is part of the Nevado-Filábride Complex, the deepest tectonic complex of the Internal Zone of the Betic Cordillera (Table 1). This complex underwent high-pressure eclogite facies metamorphism followed by decompression into greenschist facies conditions during the early Miocene (Platt et al. 2006). U–Pb SHRIMP dating on orthogneiss that intruded the entire lithological sequence, identified as Late Variscan, suggests that the metasedimentary sequences of the Nevado-Filábride Complex dates back to the Palaeozoic or earlier (Gómez-Pugnaire et al. 2012).

2.10 Euganean trachyte

Euganean trachyte, an early Oligocene subvolcanic porphyritic rock from the Euganean Hills in northeastern Italy, has a long history of exploitation dating back to the Neolithic period (Bianchin Citton and De Vecchi 2009) (Table 1). It was used by pre-Roman cultures, including the Venetic and Etruscan civilizations, and later by the Romans for various purposes such as millstones, mortars, cippi (milestones), steles, tombstones, sarcophagi, and paving materials like paving stones and flagstones, as well as structural elements for roads, bridges, aqueducts, and harbours (Renzulli et al. 1999; Capedri et al. 2000, 2003; Capedri and Venturelli 2003; Antonelli et al. 2004; Antonelli and Lazzarini 2012; Maritan et al. 2013; Germinario et al. 2018a, b; Bernardini et al. 2023). Its use continued extensively during the Middle

Ages and Renaissance in the architecture of churches, monasteries public buildings, gates, and city walls. More than a hundred quarries have been identified in the Euganean Hills (Calvino 1966), with the stones often exhibiting similar characteristics that complicate provenance identification. To address this, researchers have proposed specific geochemical, petrographic, and textural criteria to help determine the source quarry of archaeological samples (Capedri et al. 2000; Germinario et al. 2018a, b). The petrophysical and mechanical properties of the main varieties of Euganean trachyte, and the implications on decay under salt crystallisation and hydrolytic attack, have been discussed by Germinario et al. (2017a) and Lazzarini et al. (2008), respectively, while Germinario et al. (2017b) explored the impact of pollution on trachyte deterioration in urban environments.

2.11 Tønsberg latite and tønsbergite

Two igneous rocks were selected from the Tønsberg area in Norway, one of the pilot sites of the Hyperion Project. Specifically, the study considered a reddish-pink latite containing large, typically rhomb-shaped anorthoclase phenocrysts, and a tønsbergite, a red, quartz-bearing variety of larvikite, which is classified as a type of syenite or monzonite containing rhomb-shaped ternary feldspars, Ti-augite, kaersutite, and biotite (Schou-Jensen & Neumann 1988; Andersen et al. 2008; Heldal et al. 2015). These rocks formed in the late Carboniferous during the main rifting stage of the Carboniferous–Permian Oslo Graben (Neumann et al. 2004), which cuts through the Precambrian Fennoscandian Shield (Table 1). This period saw significant magmatic activity, including the eruption of "rhomb porphyry" (trachyandesite, latite) and the intrusion of the largely monzonitic Larvik composite pluton. Both rock types have been extensively used in architecture, with notable examples including the Slottsfjell tower in Tønsberg (Shabani et al. 2022) and the main lodge building of the Norwegian Order of Freemasons in Oslo (Andersen et al. 2008).

3 Methods

The selected stone materials were studied by a comprehensive petrographic and physical–mechanical characterization, as detailed below. The following description outlines the methods applied, and for the technical tests, also specifies the number of specimens tested for each stone variety.

The petrographic and textural characteristics were examined under a Leitz LABORLUX 12 POL S polarised-light optical microscope equipped with a Leica MC170 HD digital camera. Samples were prepared as 30 µm-thick thin sections. Texture evaluation was further supported by digital image analysis (DIA). A scan of each thin section was performed in both plane-polarised and cross-polarised light, using a Canon Scan SS4000US scanner equipped with a system of two rotatable polarisers, allowing the acquisition of both types of images (similar to an optical microscope).

The image obtained were 5888×4000 pixels in size with a resolution of 4000 pixels per inch. DIA was then performed to obtain areal and geometric information on the different portions of the stone (e.g. porosity, micritic or sparitic areas, and crystal size in crystalline materials). For this purpose, the free software ImageJ 1.44i (IJ) (National 275 Institute of Health, USA) was used. The segmentation procedure followed these steps (Piovesan et al. 2023a):

- conversion of photomicrographs to 8-bit images, changing from RGB colour to greyscale (256 grey channels);
- brightness and contrast adjustments to enhance the portions to be segmented;
- manual segmentation to create a binary image for the various texture types;
- for crystalline marbles, manual recognition (tracing) of each crystal to obtain precise data on crystal dimensions;
- quantification of the different textural components in terms of area percentage and measurement of the geometric parameters of the crystals (i.e., max and min Feret diameters as crystal dimensions).

Mineralogical analyses were further supported by X-Ray powder diffraction (XRPD) performed on samples prepared as fine powder using a hand mortar. XRPD was conducted using a Panalytical Empyrean diffractometer in Bragg–Brentano reflection geometry, with CuKα radiation (operating at 40 kV and 40 mA) and an X'Celerator detector. Qualitative analysis of diffraction data was carried out with X'Pert HighScore Plus® software (PANalytical) and the PDF-2 database. The reference intensity ratio (RIR) method was used to semi-quantify the phases identified in the multiphase XRPD patterns.

Open porosity, pore-size distribution, bulk density, and matrix density were measured by MIP using a Thermo Scientific Pascal 140–240 porosimeter, covering a pore radius range of 0.003–100 µm, on samples with a volume of about 1.5 cm^3. For each rock type three samples were measured. The value reported as result is the average by these three MIP measurements. The capillarity water absorption coefficient and unforced/forced water absorption were determined according to the standards EN 15801:2010 and UNI EN 1925 (2000), respectively, using cubic samples with 50 mm edges (three samples per stone type).

Hygroscopic water adsorption and desorption were measured on three 5-cm cubic samples according to the EN ISO 12571 (2000) standard. The specimens were oven-dried and then placed in an environmental chamber at

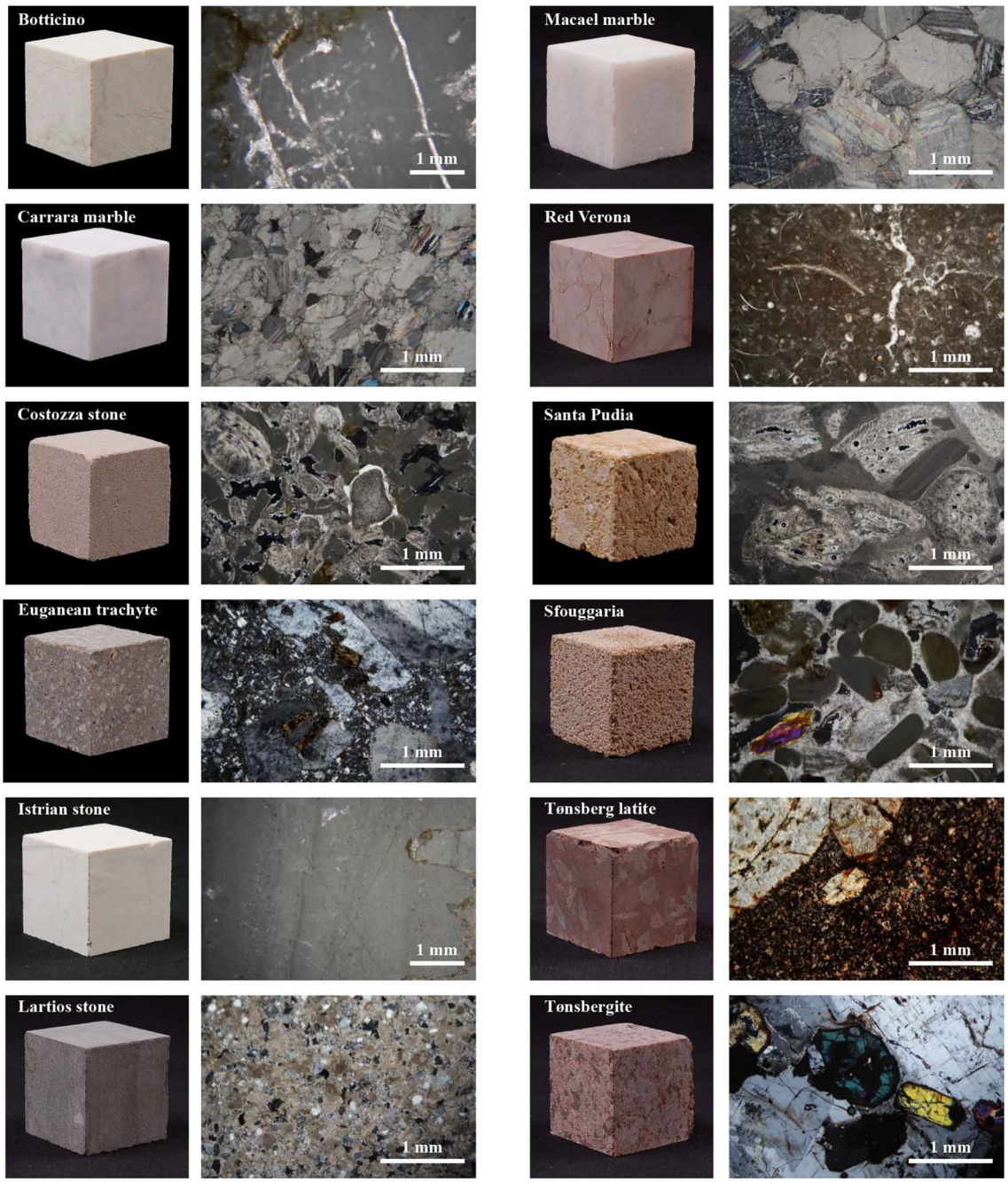

Fig. 1 Cubic specimen of the stones and their relative photomicrographs of representative thin sections observed under crossed polarized light

23 °C with relative humidity (RH) increasing in steps of 30–50–70–75–80–85–90–95%, and then decreasing in the same sequence. The samples mass was recorded at each step after equilibration at constant RH.

Water vapour diffusion was tested on three disk-shaped samples (6-cm diameter, 1-cm thickness) according to the EN ISO 12572 (2001) standard. The specimens were oven-dried and placed in an environmental chamber at 23 °C and 50% RH, using the wet-cup test with distilled water, producing a vapour flow through the specimen from the inside of the sample holder (100% RH) to the outside (50% RH).

Thermal conductivity, heat capacity, and thermal diffusivity were measured with a portable Applied Precision Isomet 2114 device, following the transient line source method (Kušnerová et al. 2013) with an accuracy of about 5% for thermal conductivity.

Table 2 Semi-quantitative mineral composition

Minerals Lithology	Cal	MgCal	Dol	Qz	Pl	K-Fs	Ano	Bt	Chl	WM	Cpx	Amp
Botticino	**xxx**		**xx**									
Carrara marble	**xxx**		**x**	**								
Costozza stone	**xxx**											
Euganean trachyte				**x**	**xx**	**x**	**xx**	**			**x**	**x**
Istrian stone	**xxx**											
Lartios stone	**xx**			**xx**	**x**				**x**	**x**		
Macael marble	**xxx**	**								**x**		
Red Verona	**xxx**			**								
Santa Pudia	**xxx**			**								
Sfouggaria	**xxx**			**x**								
Tønsberg latite					**xxx**	**x**		**			**	
Tønsbergite					**xxx**	**x**		**			**	

Mineral abbreviations after (Warr 2021)

Amp Amphibole, *Ano* Anorthoclase, *Bt* Biotite, *Cal* Calcite, *Chl* Chlorite, *Cpx* Clinopyroxene, *Dol* Dolomite, *Kfs* K-feldspar, *Qz* Quartz, *Pl* Plagioclase

Additions: *WM* white mica, and *MgCal* Magnesium rich calcite

xxx = very abundant, xx = abundant, x = medium, ** = scarce

The compressive strength, tangent Young's modulus, and tangent Poisson's ratio were determined through uniaxial compressive strength (UCS) tests following ASTM D7012-14 (2017), conducted on cylindrical specimens with a diameter of 37 mm and a length of 75 mm. A stress rate of 1 MPa/s was applied, with strains recorded using Tokyo Measuring Instruments Lab strain gauges (three 30 mm axial sensors and one 90 mm transverse sensor per specimen).

Ultrasound wave propagation was measured using an EPOCH650® Ultrasonic Flaw Detector (Olympus) with the direct transmission method (EN 14579:2004 standard). P-wave and s-wave velocities were recorded along three orthogonal axes for each specimen, using 1 MHz transducers over a circular contact surface of 3 cm in diameter. A viscoelastic ultrasound eco-gel was used for proper coupling between the transducers and the stone surfaces. Poisson's coefficient (ν), and Young's modulus (E), shear modulus (G), and bulk modulus (K) were calculated from P-wave and S-wave velocities (Guydader and Denis 1986) using the bulk density values obtained from MIP.

Durability under accelerated ageing conditions was evaluated through cyclic salt crystallization and freeze–thaw tests on three 5-cm cubic samples. Resistance to salt crystallization was assessed following the EN 12370 (1999) standard through 100 ageing cycles, each consisting of 2 h of total immersion in a 14% Na_2SO_4 aqueous solution, 16 h of drying at 105 °C, and 2 h of cooling. Resistance to freeze–thaw cycles was assessed following the EN 12371 (2001) standard, with 100 cycles consisting of freezing in air (−20 °C for 6 h) and thawing in water (6 h at room temperature). Throughout both tests, changes in sample mass, P-wave and S-wave velocities, and state of conservation were monitored.

4 Results

4.1 Petrographic and textural description

Botticino stone is a compact micritic limestone (Fig. 1) consisting of very fine-grained calcite crystals (< 4 μm) and abundant sparry dolomite crystals, mainly clustered in iso-oriented veins. XRPD analysis confirms the predominance of calcite, with dolomite present in minor quantities (Table 2). The stone features frequent stylolites along which small amounts of clay minerals and iron hydroxides are present. The rock primarily comprises a micritic matrix, locally with sparitic calcite cement. Allochemical components consist exclusively of globigerinoides. The stone can be classified as micrite according to Folk (1962), or as a mudstone according to Dunham (1962).

Carrara marble is a pure fine-grained calcitic marble with a maximum grain size (MGS) of 0.66 mm (Table 3). It exhibits a predominantly homeoblastic mosaic microstructure (Fig. 1), composed of calcite crystals with straight and curved boundary shapes, rarely forming triple junctions at 120°. The only accessory minerals observed are rare particles of carbonaceous matter and opaque minerals. XRPD analysis revealed a partially dolomitic composition with traces of quartz (Table 2).

Table 3 List and description of the texture groups classifying the stones

Texture group	Description	Grain size	Representative thin-section photomicrographs	Stone
Micritic	Mainly micritic (< 4 μm) made of very fine-grained crystals (calcite). Rarely some veins of coarser-grain size calcite are present	< 4 μm	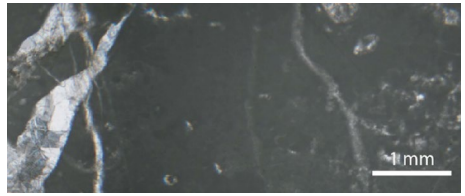	Botticino Red Verona Istrian Stone
Sparitic/Micritic	Coexistence of micritic (< 4 μm) and sparitic grain size both in fossils fillings (F) (mud or cement) or as binder (B) (matrix or cement)	Micritic (F) Sparitic (F + B) Micritic (F) Sparitic (B + clasts) Micritic (F) Sparitic (F + B) Micritic (B) Sparitic (F)	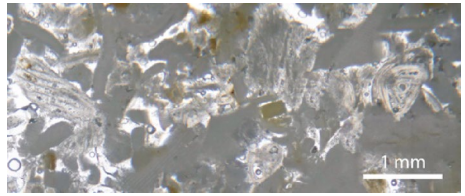	Costoza Stone Lartios stone Sfouggaria Santa Pudia
Crystalline granofelsic	Holocrystaline, heteroblastic, mosaic-like, sometimes with 120° triple junctions	0.1–0.7 mm 0.3–1.6 mm	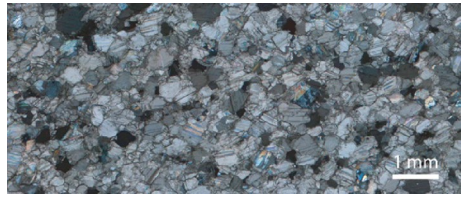	Carrara marble Macael marble
Porphyritic	Aphanitic with phenocrysts (Phc) fluctuating in a microcrystalline or partially vitreous groundmass	1–6 mm (Phc) 5–30 mm (Phc)	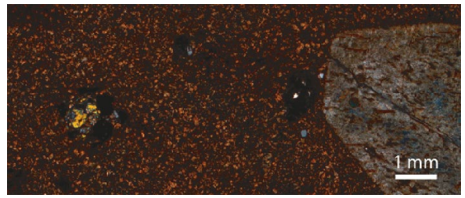	Euganean trachyte Tønsberg latite
Holocrystalline	Phanerocrystalline, holocrystalline, equigranular, hypidiomorphic, coarse-grained	5–10 mm	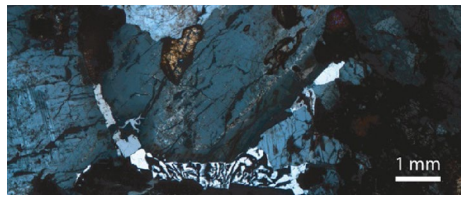	Tønsbergite

Costozza stone is a fossiliferous carbonate rock with a grain-supported texture, poorly cemented by sparitic calcite, containing subordinate micritic mud (Fig. 1). Allochems include articulated coralline algae, benthic foraminifera (mainly Miliolids and Nummulites), bryozoans, echinoderms, and molluscs. The primarily calcitic composition is enriched with iron hydroxides of a limonitic-goethitic nature, giving the stone its characteristic yellowish colour. XRPD analysis confirmed the presence of calcite only (Table 2). The stone can be classified as packed biosparite according to Folk (1962), and as packstone to grainstone rich in iron hydroxides according to Dunham (1962).

Euganean trachyte displays a holocrystalline, glomeroporphyritic, pilotaxitic texture (Fig. 1) with a microcrystalline groundmass, mainly composed of lath-shaped anorthoclase, sanidine, and plagioclase microlites, which are often interwoven in irregular unoriented fashion. Phenocrysts constitute approximately 40% of the rock and are represented by plagioclase, anorthoclase, sanidine, biotite, brown amphibole, pyroxene, and opaque minerals. Glomeroporphyritic aggregates are rare and comprise millimetric plagioclase crystals up to 6 mm in size (Table 3). The complete mineralogical composition, confirmed by XRPD data (Table 2), includes plagioclase, anorthoclase, K-feldspar (sanidine), biotite, clinopyroxene (augite), amphibole (kaersutite), and quartz as essential minerals, with apatite, zircon, magnetite, opaque minerals, and rutile as accessory minerals.

Istrian stone is a compact sedimentary rock composed almost entirely of a micritic matrix (Fig. 1) consisting of very fine-grained calcite crystals (< 4 μm) (Table 3). The texture frequently exhibits iso-oriented veins and small nuclei or irregular cavities (fenestrae) filled with secondary sparry calcite. Stylolites and sedimentary joints are common, often with small deposits of clay minerals and iron oxides and hydroxides (hematite, limonite) along them, coloured red or yellow-ochre. Allochemical components are extremely rare, consisting exclusively of bivalves or featureless fossil fragments. XRPD analysis confirmed the presence of calcite only (Table 2). The stone can be classified as micrite according to Folk (1962) and as mudstone according to Dunham (1962).

Lartios stone is a carbonate-dominated sandstone composed mainly of bioclasts (i.e., Miliolids, articulated coralline algae, echinoderms, peloids), along with grains of quartz, feldspar, chlorite, effusive magmatic rocks (basic, hyalocrystalline), and metamorphic rocks (gneiss, chlorite-bearing schist), bound by sparitic calcite cement (Fig. 1). The stone can be classified as a hybrid arenite (Zuffa 1980), containing both carbonate and siliciclastic intrabasinal clasts.

Macael marble is a medium-grained calcitic marble with a maximum grain size (MGS) of 1.57 mm. The grain

Table 4 Summary of the physical–mechanical properties measured by MIP, hydric tests (capillary sorption), hygroscopic adsorption test, water vapor test and thermal analysis

	Open porosity by MIP (vol%)	Bulk density by MIP (g/cm^3)	Matrix density by MIP (g/cm^3)	Capillary sorption (W) (g/m^2·s$^{0.5}$)	Max hygroscopic adsorption (wt%)	Water vapor resistance factor	Thermal conductivity (W/mK)	Heat capacity (MJ/m^3·K)	Thermal diffusivity ($\times 10^{-6}$ m^2/s)
Botticino	0.29	2.74	2.75	0.23	0.13	266.32	2.52	1.83	1.38
Carrara marble	0.46	2.71	2.72	0.27	0.02	222.82	3.05	2.14	1.42
Costozza stone	28.60	1.97	2.75	10.71	0.27	13.97	1.30	1.67	0.78
Euganean trachyte	7.66	2.45	2.65	1.64	0.95	69.43	1.54	1.81	0.85
Istrian stone	0.09	2.71	2.71	0.33	0.06	168.45	2.97	1.99	1.49
Lartios stone	1.06	2.67	2.70	12.41	0.64	104.46	2.97	2.02	1.46
Macael marble	0.41	2.72	2.73	0.18	0.04	123.64	2.45	1.78	1.37
Red Verona	0.08	2.69	2.69	0.42	0.25	85.40	2.82	1.99	1.42
Santa Pudia	19.65	2.21	2.75	16.50	0.24	19.01	1.51	1.73	0.87
Sfouggaria	17.04	2.25	2.71	15.26	0.36	20.90	1.26	1.62	0.78
Tønsberg latite	0.82	2.65	2.67	0.86	0.55	142.40	1.93	1.84	1.05
Tønsbergite	0.43	2.72	2.73	0.58	0.27	144.25	1.76	1.71	1.03

Table 5 Uniaxial Compressive strength (UCS): compressive strength (σ, MPa), tangent Young's modulus (E, GPa), and Poisson's ratio (ν) with standard deviations in parentheses. Ultrasound test (UT): p-wave velocity (v_p, km/s), s-wave velocity (v_s, km/s), total and relative anisotropy of ultrasound velocity (ΔM and Δm), together with the indirect measures of bulk modulus (K, GPa), shear modulus (G, GPa), Young's modulus (E, GPa), and Poisson's ratio (ν)

	Uniaxial Compressive strength (UCS)						Ultrasound test (UT)							
	σ (MPa)	St.D. (σ)	E (GPa)	St.D. (E)	ν	St.D. (ν)	p-wave	s-wave	ΔM	Δm	K	G	E	ν
Botticino stone	140.75	(±16.54)	77.21	(±3.13)	0.30	(±0.01)	6.63	3.16	1	1	81.11	27.72	74.65	0.35
Carrara marble	129.15	(±13.1)	70.15	(±4.19)	0.30	(±0.02)	5.58	2.89	5	4	54.68	22.98	60.48	0.32
Costozza stone	22.27	(±8.76)	16.27	(±2.95)	0.25	(±0.08)	3.32	1.83	6	4	15.30	7.80	20.00	0.28
Euganean trachyte	130.86	(±5.83)	33.27	(±1.03)	0.29	(±0.02)	4.37	2.38	2	2	28.56	14.06	36.23	0.29
Istrian stone	106.89	(±43.56)	69.74	(±4.4)	0.35	(±0.08)	6.42	3.06	1	1	78.73	25.75	69.66	0.35
Lartios stone	82.36	(±37.58)	34.25	(±12.66)	0.19	(±0.05)	4.98	2.82	12	8	38.20	21.59	54.50	0.26
Macael marble	76.74	(±6.74)	49.09	(±6.38)	0.25	(±0.1)	4.47	2.40	22	1	33.84	15.86	41.16	0.30
Red Verona	115.22	(±22.31)	67.02	(±1.71)	0.34	(±0.08)	6.29	3.00	4	3	75.16	24.59	66.51	0.35
Santa Pudia	9.51	(±3.47)	13.12	(±3.17)	0.26	(±0.13)	3.35	1.75	8	4	16.64	7.17	18.80	0.31
Sfouggaria	13.46	(±8.94)	17.09	(±6.97)	0.26	(±0.07)	3.72	2.04	2	2	18.89	9.43	24.26	0.29
Tønsberg latite	140.95	(±15.67)	59.09	(±2.42)	0.27	(±0.03)	5.57	2.82	5	2	28.56	14.06	36.23	0.29
Tønsbergite	117.86	(±8.56)	59.79	(±3.58)	0.34	(±0.07)	5.03	2.72	2	1	42.53	20.45	52.87	0.29

boundary shapes (GBS) are predominantly curved, with some straight, in a mainly heteroblastic polygonal mosaic microstructure of calcite crystals forming 120° triple junctions (Fig. 1). Accessory minerals observed include white mica, quartz, epidote, and opaque minerals. XRPD analysis identified predominant calcite with minor white mica and traces of magnesium-rich calcite (Table 2).

Red Verona stone is a nodular limestone containing abundant bioclasts within a micritic matrix and rare sparitic cement (Fig. 1). The allochemical constituents include ammonites (macroscopic), fragments of pelagic bivalves, planktonic micro-foraminifera, and echinoderms. In addition to the predominant calcite, there are also opaque minerals (hematite), which are responsible for the stone's pinkish colour. XRPD analysis revealed predominant calcite with traces of quartz (Table 2). The stone can be classified as biomicrite with clay levels and a nodular texture according to Folk (1962), and as mudstone with a nodular texture according to Dunham (1962).

Santa Pudia stone is a fossiliferous sedimentary rock consisting of micritic calcite and limited sparitic intragranular cement. Allochems mainly comprise bioclasts (bryozoans, articulated coralline algae, echinoderms, and molluscs), with secondary intraclasts (Fig. 1). The cement occurs as infilling of fossil voids and shell replacement. Calcite is the principal mineral, with iron oxides and hydroxides of a limonitic-hematitic nature, giving the stone a yellowish-pale colour. XRPD also identified traces of quartz (Table 2). It can be classified as packed biomicrite according to Folk (1962) and as packstone according to Dunham (1962).

Sfouggaria stone is a fossiliferous limestone consisting mainly of calcareous algae scattered in sparitic cement, with micrite limited to bioclasts (Fig. 1). Main allochemical constituents include articulated coralline algae, large benthic foraminifera, bryozoans, echinoderms, and intraclasts. The principal mineral component is calcite, with widespread iron hydroxides-oxides of a limonitic-hematitic nature giving the stone its characteristic pale yellow colour. Chert and glauconite grains are also present as syngenetic minerals. XRPD revealed traces of quartz (Table 2). The stone can be classified as biosparite rich in iron oxides and hydroxides according to Folk (1962), and as grainstone rich in iron oxides and hydroxides according to Dunham (1962).

Tønsberg latite has an aphanitic, hypocrystalline, inequigranular, hiatal texture (Fig. 1). Essential minerals include K-feldspar (orthoclase), plagioclase (oligoclase), clinopyroxene, biotite, and quartz, present in the partially glassy groundmass and as phenocrysts, which make up approximately 50% of the rock (Fig. 1). This mineralogical composition was confirmed by XRPD analysis (Table 2). The largest phenocrysts are feldspars up to 30 mm in size (Table 3). The rock also contains hematite, opaque minerals, apatite, and calcite as accessory minerals, with kaolinite and sericite as secondary minerals. The stone can be classified as latite (Le Maitre et al. 2005).

Tønsbergite is characterised by a phanerocrystalline, coarse-grained, holocrystalline, equigranular, hypidiomorphic structure, featuring numerous myrmekites and perthites. The mineralogical composition includes essential minerals such as plagioclase (oligoclase), K-feldspar (orthoclase), biotite, and clinopyroxene, with opaque minerals, hematite, apatite, and calcite as accessory minerals, and kaolinite and sericite as secondary minerals (Fig. 1). XRPD analysis confirmed the abundance of the primary minerals (Table 2).

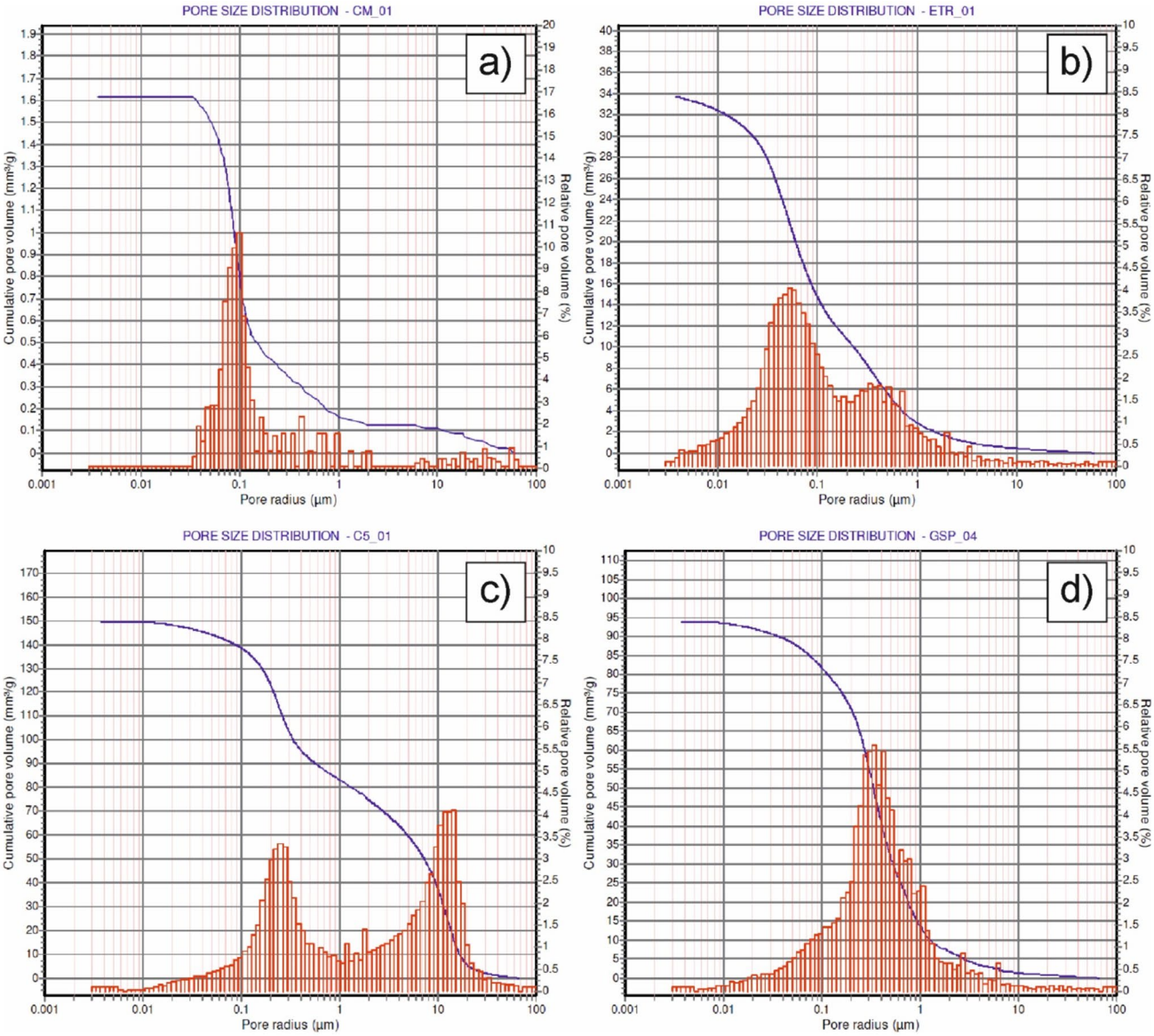

Fig. 2 Porosimetric curves (pore radius measured between 0.001 and 100 µm) of four representative samples with different pore distribution: **a** Carrara marble; **b** Euganean trachyte; **c** Costozza stone; **d** Santa Pudia stone

The stone can be classified as a monzonite (Le Maitre et al. 2005).

4.2 Texture

Based on the thin-section petrographic study combined with digital image analysis (DIA), which provided more precise data on grain size and the areal distribution of the different textures present, the different rock types were grouped into five texture classes. These classes are described and defined in Table 3.

4.3 Physical–mechanical properties

The dataset of the physical properties tested is presented in Tables 4 and 5, with graphical representations in Figs. 2 and 3. Three main groups can be identified by MIP. The first includes most of the studied materials, both carbonate and silicate rocks, which are dense (2.6–2.7 g/cm^3) and have an open porosity (ϕ_o) below approximately 1%. This group comprises Botticino stone ($\phi_o = 0.29\%$), Carrara marble ($\phi_o = 0.46\%$), Istrian stone ($\phi_o = 0.09\%$), Macael marble ($\phi_o = 0.41\%$), Red Verona stone ($\phi_o = 0.08\%$), Tønsberg latite ($\phi_o = 0.82\%$), and Tønsbergite ($\phi_o = 0.43\%$) (Table 4). The second group consists of three limestones – Costozza

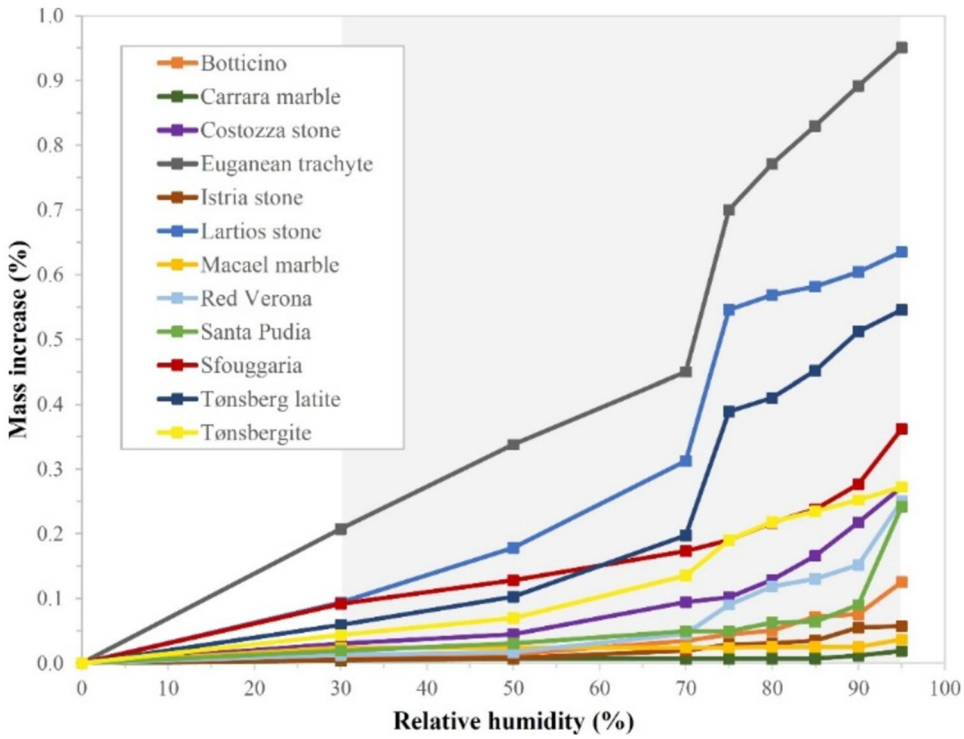

Fig. 3 Curves of hygroscopic water adsorption measured in the range 30–95% RH

stone, Sfouggaria stone, and Santa Pudia stone – with bulk density below 2.3 g/cm^3 and high porosity, ranging from 17% (Sfouggaria stone) to 29% (Costozza stone) on average (Table 3). The Euganean trachyte represents an intermediate case, with a bulk density of around 2.4 g/cm^3 and an open porosity of 7–8%.

The pore size distribution varies among the samples, consistent with differences in pore abundance. The first group, represented by Carrara marble (see Fig. 2), predominantly features small pores (mainly around 0.1 µm). In contrast, the second group, including Costozza and Santa Pudia stones (Fig. 2, bottom), exhibits a broader range of pore sizes, typically between 0.1 and 10–50 µm. The trachyte sample occupies an intermediate position, with a significant proportion of pores ranging from 0.1 to 1 µm, although less abundant than in the second group. Additionally, trachyte features a high number of very small pores, with diameters below 0.01 µm (Fig. 2). For most samples, matrix density values are close to the bulk density, except in highly porous rocks, which show matrix density higher by 0.5–0.7 g/cm^3 (e.g., Costozza stone has a bulk density of 1.97 g/cm^3 and a matrix density of 2.75 g/cm^3) (Table 4).

Hydric tests (capillary sorption) confirmed MIP results, correlating with the measured open porosity (Table 4). While the amount of absorbed water depends on the total volumetric porosity, water movement within the material is facilitated when most of the porosity falls within the capillarity size range (0.1 to 1000 µm in diameter, Klopfer 1985). The abundance of capillary pores in Costozza, Lartios, Santa Pudia, and Sfouggaria stones enhances their water absorption, with capillary sorption values exceeding 10 g/m^2·s$^{0.5}$ (Table 4). The Euganean trachyte has an intermediate value (1.64 g/m^2·s$^{0.5}$), while all other stones exhibit capillary sorption values below 1 g/m^2·s$^{0.5}$.

Regarding water vapour interaction and response to RH variations, there is a weak negative correlation between the maximum water vapour adsorption in high humidity and resistance to water vapour transmission. Stones with the high vapour resistance factors (over 100) (Table 4), such as Botticino stone, Carrara marble, Lartios stone, and Macael marble, exhibit low hygroscopic adsorption (0.1% or less mass increase at 95% RH). However, other correlations are scarce. The most porous stones (Costozza, Sfouggaria, and Santa Pudia) have low vapour resistance factors (around 20 or less) (Table 4). The mass changes due to water vapour adsorption are less predictable, as shown in Fig. 3. The Euganean trachyte records the highest mass increase at 95% RH, approximately 1% (Table 4), while for most stones (regardless of density or porosity), it is below 0.3%. This behaviour is linked to the larger fraction of micropores found in the Euganean trachyte samples here analysed. The curves knee indicates the critical stage when adsorption accelerates, usually at 70% or 90% RH, depending on the rock type. Before these humidity levels, the adsorption process is almost linear (Fig. 3). For instance, Tønsberg latite shows nearly double the water vapour adsorption from 70 to 75% RH, while Santa Pudia stone mass increase from 90 to 95% RH nearly triples (Fig. 3).

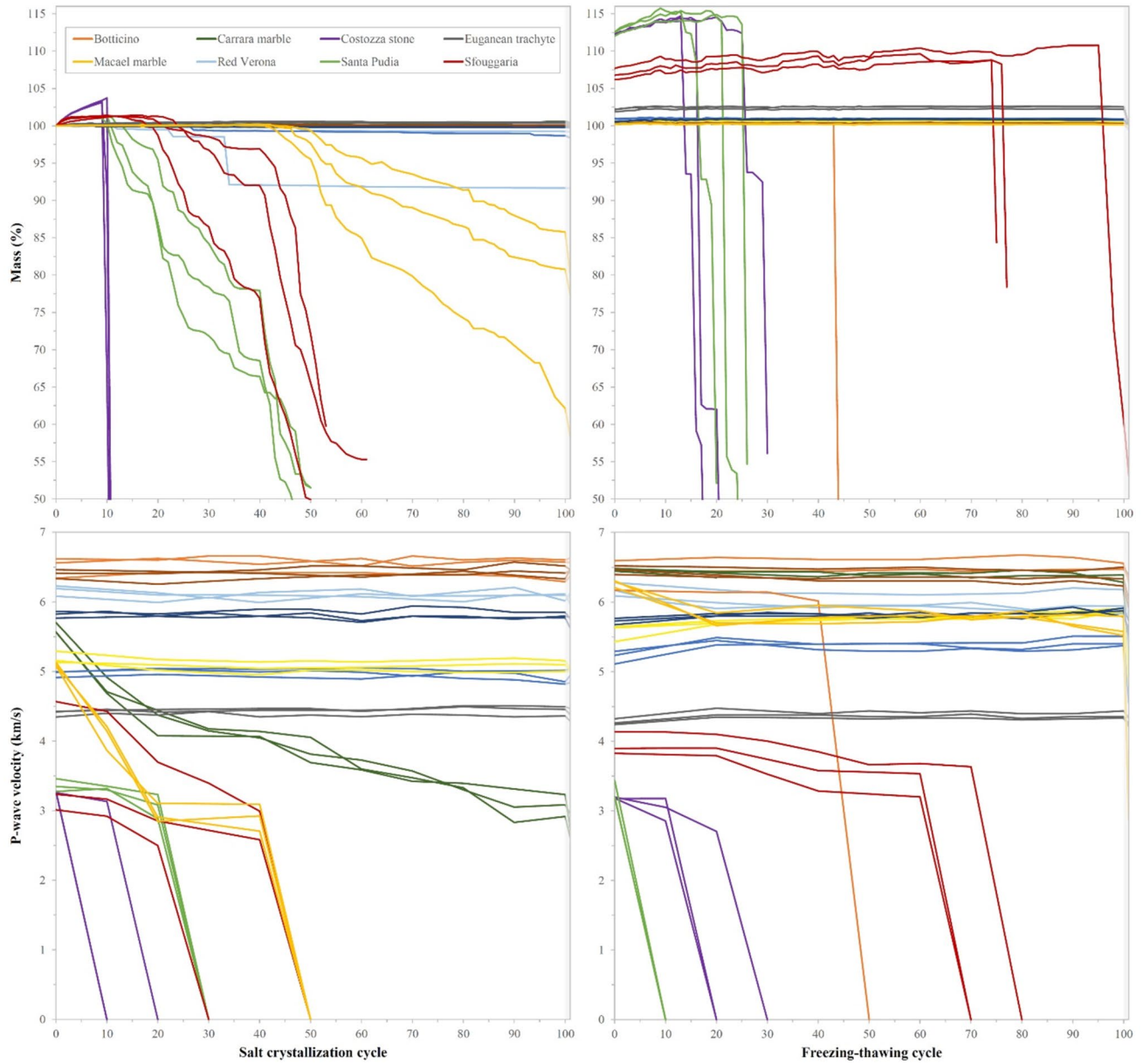

Fig. 4 Changes of mass and p-wave velocity measured on three samples for each rock type during the artificial accelerated ageing tests (the colour codes of the trends deviating from the averages are indicated in the legend). Cycle 0 and cycle 101 (shaded area) indicate: for the salt crystallization tests, the initial dry state and the final dry state of the samples after salt removal in water, respectively; for the freeze–thaw tests, the initial saturated state and the final dry state, respectively

Porosity also affects the thermal properties of these rocks, with higher porosity linked to poorer thermal performance, as shown by lower thermal conductivity (λ), heat capacity (C), and diffusivity (α). Stones with the highest porosity (Costozza, Santa Pudia, and Sfouggaria) have the lowest thermal conductivity, ranging from 1.25 to 1.51 W/mK. Carrara marble records the highest thermal conductivity (3.05 W/mK) and heat capacity (2.14 MJ/m^3·K), while Istrian stone displays the highest heat diffusivity ($\alpha = 1.49 \times 10^{-6}$ m^2/s). Most stones have low thermal diffusivity (0.78 to 0.87×10^{-6} m^2/s). The volcanic rocks (Euganean trachyte and Tønsberg latite) and Tønsbergite show intermediate thermal conductivity (1.5 to 2 W/mK). Marbles (Macael and Carrara), compact limestones (Botticino, Istrian, Red Verona), and Lartios sandstone exhibit the highest thermal conductivity (2 W/mK) and diffusivity ($> 1.3 \times 10^{-6}$ m^2/s) (Table 4). These results align with mean values reported in the literature (Clauser and Huenges 1995; Clauser 2011; Pimienta et al. 2018; Coletti et al. 2021). Since the stones do not contain significant

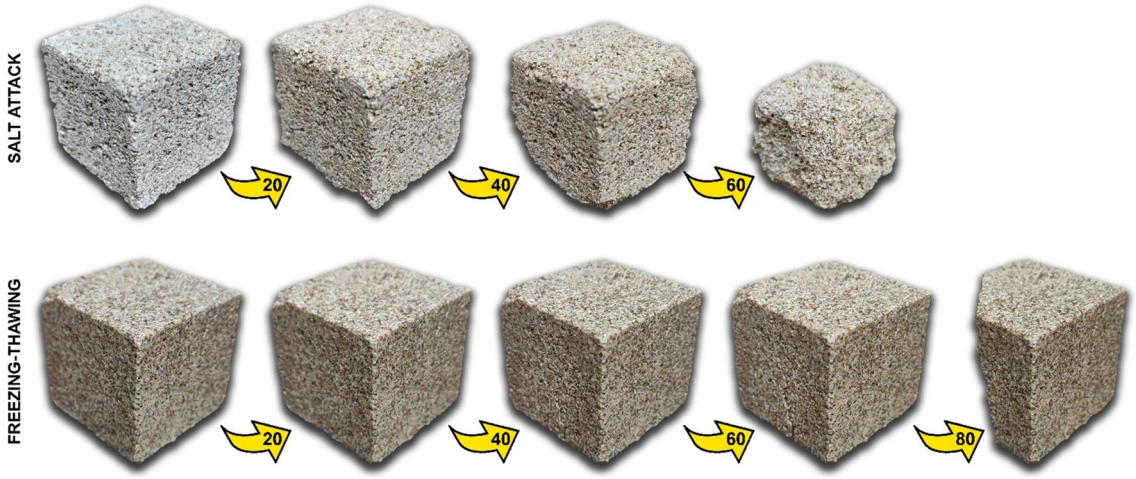

Fig. 5 Deterioration evolution observed on samples of Sfouggaria stone during the ageing tests at 20 cycle steps

amounts of high-thermal-conductivity minerals like quartz (Horai 1971; Clauser and Huenges 1995), thermal behaviour is mainly governed by pore abundance, particularly pores > 0.1 µm (Giraud et al. 2007; Pimienta et al. 2018). Table 5 shows the mechanical strength and deformability characteristics of the stones studied. Most materials show good to excellent mechanical performance, with compressive strengths (σ) generally exceeding 100 MPa (and even 150 MPa in some cases). Mechanical behaviour is closely linked to porosity, as the three most porous stones (Costozza, Sfouggaria, and Santa Pudia) exhibit low compressive strengths (10–22 MPa on average) and Young's modulus values ranging between 13 and 17 GPa, with Poisson's ratio from 0.19 and 0.35.

Comparisons with ultrasound tests reveal that p-wave and s-wave velocities vary with porosity range found by MIP. The most porous and least rigid stones show the lowest values – around 3.5 km/s for p-waves and 2 km/s for s-waves. Carrara marble has the highest velocities (6.63 and 3.16 km/s for p- and s-waves, respectively), while other stones fall within an intermediate range.

Most analysed samples show minimal to low total (ΔM) and relative anisotropy (Δm), with values around 1 or below 5%. Macael marble and Lartios stone exhibit the highest total anisotropy (ΔM = 22 and 12, respectively) (Table 5), with Lartios stone also showing structural relative anisotropy (Δm = 8). Indirect calculation of physical–mechanical parameters – such as bulk modulus (K), shear modulus (G), Young's modulus (E), and the Poisson's ratios (ν) – based on ultrasonic tests confirm the weakest resistance of high-porosity stones, consistent with UCS-measured properties (Table 5). Botticino stone has the highest bulk, shear, and Young's moduli (K = 81.11 GPa; G = 27.72 GPa; E = 74.65 GPa), while the weakest stones (Costozza, Sfouggaria, and Santa Pudia) show the lowest values (K~ 15–18 GPa; G~ 7–9 GPa; E~ 18–24 GPa; Table 5).

4.4 Decay during artificial ageing

The stone materials tested exhibit different resistance to artificial accelerated ageing, influenced by their inherent rock properties and the experimental conditions. The results are summarised in the graphs of Fig. 4, which show how mass and p-wave velocity change with respect to the deterioration degree. Salt-induced decay generally progresses more rapidly than freeze–thaw decay; salt crystallisation primarily causes disintegration and rounding, whereas freeze-thawing results in fracturing and microcracking, with sample edges remaining sharp (Fig. 5).

During the salt crystallization tests, the stones significantly affected by weight loss include Costozza, which withstands approximately 10 ageing cycles before rapid decay through powdering and blistering; Santa Pudia and Sfouggaria, which exhibit pronounced decay starting between the 20th and 40th cycles and reaching a critical stage around the 50th cycle, characterised by crumbling, rounding (see Santa Pudia changes during salt cycles in Fig. 5), and differential erosion; and Macael marble, which remains stable for the first 50 cycles but then undergoes substantial decay through sugaring and microcracking, resulting in a 20% to 40% weight loss by the end of the programme. The remaining stones show minimal impact (except for minor detachments due to pre-existing fractures), though differential erosion and delamination are noticeable on Red Verona and Lartios stones, respectively, most probably because of their specific sedimentary textures.

The variations in p-wave velocity during the salt crystallization tests align with the mass changes, particularly revealing early signs of physical–mechanical decay in marbles

before visible deterioration occurs. For instance, Macael shows a 40% reduction in p-wave velocity by the 50th cycle, despite minimal visible decay, while Carrara experiences an early, gradual decrease, culminating in a 50% reduction in p- and s-wave velocities by the test conclusion.

During the freeze-thawing tests, Costozza, Santa Pudia, and Sfouggaria stones again exhibit the least durability due to pervasive fracturing, sudden large detachments, and minor disintegration. Costozza and Santa Pudia undergo rapid and substantial decay between the 15th and 30th cycles (see Santa Pudia freeze–thaw behaviour in Fig. 5), while significant detachments in Sfouggaria stone commence around the 70th cycle. Macael and Carrara marbles sustain no major weight loss throughout the testing period, however, p-wave velocity measurements detect subtle decay, associated with increasing porosity: by the end, Macael shows 40% decrease in p-wave velocity and 20% decrease in s-wave velocity, while Carrara shows 15% and 10%, respectively. The other stones do not exhibit notable physical–mechanical variations.

It is notable that Santa Pudia is the only stone demonstrating lower durability to freeze–thaw decay than to salt-induced decay.

5 Discussion

Comparing petrographic observations with quantitative measurements of physical properties, including porosity, permeability, and vapour permeability, highlights the significance of pore size distribution data for understanding potential stone decay processes. Mercury Intrusion Porosimetry (MIP) analysis, conducted to characterise open porosity, categorised the twelve studied stones into three groups: very low (below 1%), low-to-medium (from 1% to 7–8%), and high porosity (15% to 30%). The high-porosity group includes Costozza, Sfouggaria, and Santa Pudia stones. Euganean trachyte displays medium porosity, while all other stones fall within the very low-porosity group. This classification is also evident in the pore size distribution curves. The very low-porosity stones (including the two marbles, compact limestones, and Norwegian silicatic rocks) show a pore radius distribution centred around 0.1 μm (as seen in Carrara marble, Fig. 2), whereas other types display a broader distribution. The three rocks with the highest porosity have pores predominantly distributed in the range of 0.1 to 10–50 μm, with an evident dominance of pores below the critical 1 micron radius threshold. This pore range significantly affects water interaction, particularly capillarity, as these stones exhibit the highest water absorption capacity due to capillary rise, and also influence negatively their capacity to resist to salt crystallization and freeze–thaw cycles.

Larger pore sizes, on the contrary, influence the thermal behaviour of the rocks, generally aligning with porosity trends: higher porosity correlates with lower thermal properties, particularly thermal conductivity and diffusivity. Similarly, there is a strong correlation between uniaxial compressive strength (UCS) and ultrasonic testing (UT) parameters, with the highest open porosity. Interaction with relative humidity (RH), on the other hand, is governed by pore size. The highest hygroscopic sorption is found in Euganean trachyte, followed by Lartios stone and Tønsberg latite, which contain the highest number of micropores conducive to condensation (Ruedrich et al. 2011). The two marbles display the lowest variation. Stones with larger pore radii exhibit lower vapour diffusion resistance, allowing easier moisture movement within the stone. This characteristic can significantly affect the stone susceptibility to decay mechanisms related to moisture.

Laboratory ageing tests, involving freeze–thaw and salt cycles, assess stone durability under conditions of frost and both sub- and efflorescence-driven salt crystallisation. These tests simulate the environmental stresses that stones may encounter in real-world settings, providing valuable insights into their long-term durability and resistance to decay processes. Decay phenomena vary according to specific rock physical properties. In porous stones, ice or salt crystal growth within (meso and micro-) pores led to notable decay due to crystallisation pressure during ageing cycles. During salt crystallisation tests, Costozza stone exhibits the fastest decay through powdering and blistering, followed by the other two high-porosity rocks, Santa Pudia and Sfouggaria stones. Macael marble also undergoes significant sugaring and material loss (with ultrasound monitoring detecting early internal cracks that were not visually observable), showing markedly different behaviour from the fine-grained Carrara marble.

Freeze–thaw tests are generally less damaging than salt crystallisation over cycles. However, the stones with the highest porosity – Costozza, Santa Pudia, and Sfouggaria – remain the most vulnerable in these tests.

6 Conclusions

This study investigated the physical–mechanical properties and durability of various rock types employed in prominent European cultural heritage monuments and buildings, selected as pilot sites within the European Hyperion project. The rocks examined are primarily those used in the pilot sites of the project, located in Venice (Italy), Rhodes (Greece), Granada (Spain), and Tønsberg (Norway). This comprehensive set comprises twelve rock types: six limestones (Botticino, Red Verona, and Costozza stones from

Italy; Istrian stone from Croatia; Sfouggaria stone from Greece; Santa Pudia stone from Spain), one carbonate-dominated sandstone (Lartios stone from Greece), two white marbles (Carrara marble from Italy and Macael marble from Spain), two volcanic rocks (Euganean trachyte from Italy and Tønsberg latite from Norway), and one intrusive igneous rock (tønsbergite from Norway). Together, these rocks offer a representative overview of materials commonly used across some renowned European architectural-artistic heritage sites. Furthermore, their distinct petrographic features can serve as a proxy for similar materials not directly considered in this study but sharing analogous characteristics (e.g., mineralogy, compactness, porosity) and behaviour (e.g., water interaction or durability under ageing tests).

The results highlight the decisive influence of pore structure and porosity on durability of the stones. High-porosity stones, including Costozza, Sfouggaria, and Santa Pudia, demonstrated significant susceptibility to salt crystallisation and freeze–thaw processes, making them particularly vulnerable in environments characterised by water-related stresses or thermal cycling. The findings also underline the relationship between porosity, vapour permeability, and thermal properties, which play a decisive role in stone performance under varying environmental conditions.

The pilot sites studied—Venice, Rhodes, Granada, and Tønsberg—represent diverse climate regimes, ranging from humid subtropical and Mediterranean to continental environments. For instance, Venice faces increasing risks due to rising sea levels, frequent flooding, and salt crystallisation, which particularly impact porous materials through capillary water rise and salt transport. In Rhodes, salt-laden marine aerosols contribute to salt crystallisation, accelerating decay processes in vulnerable stones like Sfouggaria limestone and Lartios sandstone. Granada experiences freeze–thaw cycles and thermal stress due to its continental Mediterranean climate and significant diurnal temperature variations, posing risks to stones with high water absorption capacity or poor thermal diffusivity. Tønsberg, with its cold, humid continental climate, is subject to prolonged frost action, biological growth, and rainwater-driven weathering, which particularly threaten highly porous and moisture-sensitive stones.

Given the increasing impacts of climate change, such as rising temperatures, more extreme precipitation, and changes in the frequency of freeze–thaw cycles, these environmental stressors are expected to exacerbate stone decay mechanisms. The observed decay patterns in this study can serve as a foundation for predicting how such materials might respond to future climate scenarios.

While detailed recommendations for site-specific risk assessments, preventive and adaptive preservation strategies, monitoring approaches, and material substitution lie beyond the scope of this study, such strategies fundamentally rely on a thorough understanding of the mechanical, physical–chemical, textural, and hygrothermal properties of stone materials. This work provides essential data on these properties, serving as a foundation for future studies aimed at developing targeted conservation solutions tailored to specific environmental conditions. Specifically, this study highlights the critical role of pore size distribution in determining the decay behaviour and durability of building, sculptural and decorative stone types used in cultural heritage, with applicability extending to a broader range of rocks in architectural contexts. Moreover, vapour permeability data, combined with factors such as porosity and pore size distribution, are essential for evaluating the hygrothermal behaviour of stones, influencing their performance and durability in historic heritage structures.

Acknowledgements This work was carried out thanks to the funding provided by the HYPERION project supported by the European Union's Framework Programme for Research and Innovation (Horizon 2020) under Grant Agreement number 821054.

Authors contributions All authors contributed to the study conception and design. Data collection and analysis were performed by C.C., L.G., R.P., F.A., and E.T.. The first draft of the manuscript was written by C.C., L.G., C.M., R.P., F.A., and E.T.. All authors commented on previous versions of the manuscript. All authors read and approved the final manuscript.

Funding Horizon 2020 Framework Programme, 821054.

Data availability No datasets were generated or analysed during the current study.

Declarations

Conflict of interest The authors declare no competing interests.

References

Albertini G (1991) Geologia dei marmi veronesi. I Marmi a Verona. 254:28–42

Alcalde M, Martin L, Bello MA, Martin A (1992) Macroscopical morphology of deterioration of the stone used in the cathedral whole of Granada/Spain. Mater Constr 42(226):27–48. https://doi.org/10.3989/mc.1992.v42.i226.710

Andersen T, Trønnes RG, Nilsen O, Larsen AO (2008) Alkaline rocks of the Oslo Rift SE Norway: a field trip with emphasis on felsic to intermediate intrusive rocks and their associated

mineralizations. Eurogranites 2008/IGCP 510 Field Trip August 1st to 5th, 2008 2465:54
Antonelli F, Lazzarini L (2012) The first archaeometric characterization of Roman millstones found in the Aquileia archaeological site (Udine, Italy). Archaeometry 54(1):1–17. https://doi.org/10.1111/j.1475-4754.2011.00615.x
Antonelli F, Lazzarini L (2013) The use of white marble in the central and upper adriatic between greece and rome: hellenistic stelae from the necropolis of ancona (Italy). Camb Archaeol J 23(2):149–162. https://doi.org/10.1017/S0959774313000231
Antonelli F, Lazzarini L (2015) An updated petrographic and isotopic reference database for white marbles used in antiquity. Rend Fis Acc Lincei 26(4):399–413. https://doi.org/10.1007/s12210-015-0423-4
Antonelli F, Bernardini F, Capedri S, Lazzarini L, Montagnari Kokelj E (2004) Archaeometric study of protohistoric grinding tools of volcanic rocks found in the Karst (Italy-Slovenia) and Istria (Croatia). Archaeometry 46(4):537–552. https://doi.org/10.1111/j.1475-4754.2004.00172.x
Antonelli F, Savalli A, Cantisani E, Fratini F, Giamello M, Lezzerini M, Pecchioni E, Tesser E (2016) Multianalytical approach to diagnosis and conservation of building materials: the case of Punta Troia Castle in Marettimo (Aegadian Islands—Sicily, Italy). Appl Phys A Mater Sci Process 122(4):264. https://doi.org/10.1007/s00339-016-9803-6
Apostolopoulou M, Keramidas V, Galanaki N, Kalofonou M, Skoula C, Karoglou M, Delegou E, Mouzakis C, Bakolas A, Moropoulou A, Pikoula M, Kalagri A, Farmakidou E, Michailidou M (2019) A study on the historical materials of the Apollo Pythios Temple in Rhodes and the evaluation of potential restoration materials. Heritage 2:988–1022. https://doi.org/10.3390/heritage2010065
Archibald Z (2013) The aegean Islands (Prehistoric to Roman). Archaeological Rep, Archaeol Greece 2012–2013:76–95
Arizzi A, Viles H, Cultrone G (2012) Experimental testing of the durability of lime-based mortars used for rendering historic buildings. Constr Build Mater 28:807–818. https://doi.org/10.1016/j.conbuildmat.2011.10.059
ASTM D7012-14 (2017) Standard test methods for compressive strength and elastic moduli of intact rock core specimens under varying states of stress and temperatures. Book of Standards Volume 04.09, Subcommittee D18.12. https://doi.org/10.1520/D7012-14
Bairami K (2017) Large scale rhodian sculpture of hellenistic and roman times. Archaeopress, NY, Access Archaeology, p 892
Bairami K (2023) Sculpture from 'Pantheon': An open-air sanctuary at the foothills of the Rhodian acropolis. In: Stefanakis MI, Mavroudis G, Seroglou FK (eds) Religion and Cult in the Dodecanese during the first Millennium BC. Archaeopress, NY, pp 93–104
Bello MA, Martin L, Martin A (1992) Microchemical identification of Macael white marble in some spanish monuments. Mater Constr 42(225):23–30. https://doi.org/10.3989/mc.1992.v42.i225.718
Benchiarin S (2007) Carbonate lithotypes employed in historical monuments: quarry materials, deterioration and restoration treatment. PhD Thesis, University of Padova.
Bernardini F, Velicogna M, De Min A, Antonelli F, Gambacurta G, Bressan D, Fabec T (2023) Euganean trachytic grinding stones in the caput adriae from the iron age to the roman period: reassessment of the protohistoric quarries. Archaeometry 65(3):445–462. https://doi.org/10.1111/arcm.12835
Berto L, Favaretto T, Saetta A, Antonelli F, Lazzarini L (2012) Assessment of seismic vulnerability of art objects: The "Galleria dei Prigioni" sculptures at the Accademia Gallery in Florence. J Cult Herit 13(1):7–21. https://doi.org/10.1016/j.culher.2011.06.005
Bianchin Citton E, De Vecchi G (2009) L'impiego della trachite euganea nella fabbricazione di macine in età preromana. In: Rossi ES, Zanovello P (eds) E Bianchin Citton Dinamiche insediative nel territorio dei Colli Euganei dal Paleolitico al Medioevo. Atti del convegno di studi. Este & Monselice, Italy, pp 139–150
Bonazza A, Messina P, Sabbioni C, Grossi CM, Brimblecombe P (2009a) Mapping the impact of climate change on surface recession of carbonate buildings in Europe. Sci Total Environ 407:2039–2050. https://doi.org/10.1016/j.scitotenv.2008.10.067
Bonazza A, Sabbioni C, Messina P, Guaraldi C, De Nuntiis P (2009b) Climate change impact: mapping thermal stress on carrara marble in europe. Sci Total Environ 407:4506–4512. https://doi.org/10.1016/j.scitotenv.2008.10.067
Borghi A, Berra V, D'Atri A, Dino GA, Gallo LM, Giacobino E, Martire L, Massaro G, Vaggelli G, Bertok C, Castelli D, Costa E, Ferrando S, Groppo C, Rolfo F (2015) Stone materials used for monumental buildings in the historical centre of Turin (NW Italy): architectonical survey and petrographical characterization of Via Roma. Geol Soc London Special Publicat. https://doi.org/10.1144/SP407.20
Braga G (2004) Le pietre naturali da costruzione della città di Padova. Cleup, Padova
Bruno M, Attanasio D, Prochaska W (2015) The docimium marble sculptures of the grotto of tiberius at sperlonga. Am J Archaeol 119(3):375–394. https://doi.org/10.3764/aja.119.3.0375
Calvino F (1966) Le cave dei Colli Euganei. Padova: Consorzio per la valorizzazione dei Colli Euganei.
Capedri S, Venturelli G (2003) Trachytes employed for funerary artefacts in the roman colonies regium lepidi (Reggio Emilia) and Mutina (Modena) (Italy): Provenance inferred by petrographic and chemical parameters and by magnetic susceptibility. J Cult Herit 4:319–328. https://doi.org/10.1016/j.culher.2003.01.002
Capedri S, Venturelli G, Grandi R (2000) Euganean trachytes: Discrimination of quarried sites by petrographic and chemical parameters and by magnetic susceptibility and its bearing on the provenance of stones of ancient artefacts. J Cult Herit 1:341–364. https://doi.org/10.1016/S1296-2074(00)01091-8
Capedri S, Grandi R, Venturelli G (2003) Trachytes used for paving Roman roads in the Po Plain: characterization by petrographic and chemical parameters and provenance of flagstones. J Archaeol Sci 30:491–509. https://doi.org/10.1006/jasc.2002.0857
Clauser C (2011) Thermal Storage and Transport Properties of Rocks, II: Thermal Conductivity and Diffusivity. In: Gupta HK (ed) Encyclopedia of Solid Earth Geophysics Encyclopedia of Earth Sciences Series. Springer, Dordrecht
Clauser C, Huenges E (1995) Thermal conductivity of rocks and minerals. Rock Phys Phase Relat: a Handbook Phys Const 3:105–126
Clerici A, Meda A (2005) Confronto tra le caratteristiche meccaniche di diversi livelli di estrazione del Botticino Classico. Giornale di Geologia Applicata 2:307–312. https://doi.org/10.1474/GGA.2005-02.0-45.0071
Coletti C (2024) Climate change threats to stone cultural heritage: state of the art of quantitative damage functions and new challenges for a sustainable future. Heritage 7(6):3276–3290. https://doi.org/10.3390/heritage7060154
Coletti C, Borghi A, Cossio R, Dalconi MC, Dalla Santa G, Peruzzo L, Sassi R, Vettorello A, Galgaro A (2021) A multi-scale methods comparison to provide granitoid rocks thermal conductivity. Constr Build Mater 304:124612. https://doi.org/10.1016/j.conbuildmat.2021.124612
Corbí H, Lancis C, García-García F, Pina JA, Soria JM, Tent-Manclús JE, Viseras C (2012) Updating the marine biostratigraphy of the Granada Basin (central Betic Cordillera). Insight for the Late Miocene palaeogeographic evolution of the Atlantic-Mediterranean seaway. Geobios 45:249–263. https://doi.org/10.1016/j.geobios.2011.10.006

Cornale P, Rosanò P (1994) Le pietre tenere del vicentino: uso e restauro. Associazione Artigiani della Provincia di Vicenza Camera di Commercio Industria Artigianato Agricoltura di Vicenza, Amministrazione Provinciale di Vicenza, Consorzio Artigiani Restauratori Veneti, Vicenza.

Cultrone G, Sebastia E, Ortega Huertas M (2007) Durability of masonry systems: a laboratory study. Constr Build Mater 21:40–51. https://doi.org/10.1016/j.conbuildmat.2005.07.008

de Jong van Coevorden CM, Sánchez CC, Bretones AR, Pantoja MF, García SG, Martín RG, (2012) Nondestructive evaluation of the preservation state of stone columns in the hospital real of granada. Nondestructive Testing and Evaluation 27(4):335–351. https://doi.org/10.1080/10589759.2011.645822

Di Battistini G, Vernia L, Zucchi D, Modena M, Ronchini R (2005) Il marmo botticino classico nuovi dati sulla caratterizzazione fisico-meccanica di questo importante materiale lapideo ornamentale. L'informatore Del Marmista 44(518):25–34

Dunda S, Kujundžić T (2004) Historical review of exploitation and utilization of stone in Croatia. In: Přykril R (ed) Proceedings of the Congress "Dimension stone - new perspectives for a traditional building material". Prague, pp 29–34.

Dunham RJ (1962) Classification of Carbonate Rocks According to Depositional Texture: In Northern Iraq Arabian Gulf, Geology and Productivity. AAPG, Foreign Reprint Series

Durn G, Ottner F, Tišljar J, Mindszenty A, Barudžija U (2003) Regional subaerial unconformities in shallow-marine carbonate sequences of Istria: sedimentology, mineralogy, geochemistry and micromorphology of associated bauxites, palaeosols and pedo-sedimentary complexes. Field Trip P8, Field Trip Gidebook, 22nd IAS Meeting of Sedimentology, Opatija.

EN 12370 (1999) *Natural Stone Test Methods - Determination of Resistance to Salt Crystallisation*. CEN, Brussels

EN 12371 (2001) *Natural Stone Test Methods - Determination of Frost Resistance*. CEN, Brussels

EN 14579 (2004) Natural Stone Test Methods - Determination of Sound Speed Propagation. Brussels: CEN.

EN 15801 (2010) Conservation of cultural property - Test methods - Determination of water absorption by capillarity. Brussels: CEN.

En UNI (1925) (2000) Natural stone test methods - Determination of water absorption coefficient by capillarity. CNR-ICR, Rome

Folk RL (1962) Spectral Subdivision on Limestone Types. In: Classification of Carbonate Rocks-A Symposium, 62–84.

Foraboschi P (2017) Specific structural mechanics that underpinned the construction of Venice and dictated Venetian architecture. Eng Fail Anal 78:169–195. https://doi.org/10.1016/j.engfailanal.2017.03.004

Galanaki N, Delegou E, Bris T, Moropoulou A (2022) Accelerated ageing tests of sodium chloride for the evaluation of stones durability to salt crystallization: a comparative study of selected restoration lithotypes. Develop Built Environ. https://doi.org/10.1016/j.dibe.2022.100081

Geometrante R, Almesberger D, Rizzo A (2000) Characterization of the State of compression of Pietra d'Istria elements by non-destructive ultrasonic technique. 15th World Conference on Non-destructive Testing, Roma (Italy).

Germinario L, Siegesmund S, Maritan L, Mazzoli C (2017a) Petrophysical and mechanical properties of Euganean trachyte and implications for dimension stone decay and durability performance. Environmental Earth Sciences 76:1–21. https://doi.org/10.1007/s12665-017-7034-6

Germinario L, Siegesmund S, Maritan L, Simon K, Mazzoli C (2017b) Trachyte weathering in the urban built environment related to air quality. Heritage Science 5:44. https://doi.org/10.1186/s40494-017-0156-z

Germinario L, Hanchar JM, Sassi R, Maritan L, Cossio R, Borghi A, Mazzoli C (2018a) New petrographic and geochemical tracers for recognizing the provenance quarry of trachyte of the euganean hills. Northeastern Italy Geoarchaeol 33(4):430–452. https://doi.org/10.1002/gea.21666

Germinario L, Zara A, Maritan L, Bonetto J, Hanchar JM, Sassi R, Siegesmund S, Mazzoli C (2018b) Tracking trachyte on the Roman routes: Provenance study of Roman infrastructure and insights into ancient trades in northern Italy. Geoarchaeology 33:417–429. https://doi.org/10.1002/gea.21667

Germinario L, Coletti C, Girardi G, Maritan L, Praticelli N, Sassi R, Mazzoli C (2022) Microclimate and weathering in cultural heritage: Design of a monitoring apparatus for field tests. Heritage 5:3211–3219. https://doi.org/10.3390/heritage5040165

Germinario L, Giannossa LC, Lezzerini M, Mangone A, Mazzoli C, Pagnotta S, Spampinato M, Zoleo A, Eramo G (2023) Petrographic and chemical characterization of the frescoes by saturnino gatti (Central Italy, 15th Century). Appl Sci 13:7223. https://doi.org/10.3390/app13127223

Gheno G, Badetti E, Brunelli A, Ganzerla R, Marcomini A (2018) Consolidation of Vicenza, Arenaria and Istria Stones: a comparison between nano-based products and acrylate derivatives. J Cult Herit 32:44–52. https://doi.org/10.1016/j.culher.2018.02.013

Gil-Martín LM, Fernández-Ruiz MA, Hernández-Montes E (2022) Mechanical characterization and creep behavior of a stone heritage material used in Granada (Spain): Santa Pudia Calcarenite. Rock Mech Rock Eng 55:5659–5669. https://doi.org/10.1007/s00603-022-02946-0

Giraud A, Gruescu C, Do DP, Homand F, Kondo D (2007) Effective thermal conductivity of transversely isotropic media with arbitrary oriented ellipsoidal inhomogeneities. Int J Solids Struct 44(9):2627–2647. https://doi.org/10.1016/j.ijsolstr.2006.08.011

Gómez-Pugnaire MT, Rubatto D, Fernández-Soler JM, Jabaloy A, López-Sánchez-Vizcaíno V, González-Lodeiro F, Galindo-Zaldívar J, Padrón-Navarta JA (2012) Late Variscan magmatism in the Nevado-Filábride Complex: U-Pb geochronologic evidence for the pre-Mesozoic nature of the deepest Betic complex (SE Spain). Lithos 146–147:93–111. https://doi.org/10.1016/j.lithos.2012.03.027

Guydader J, Denis A (1986) Propagation des ondes dans les roches anisotropes sous contrainte évaluation de la qualité des schistes ardoisiers. Bull Int Assoc Eng Geol 33:49–55

Hanken N-M, Bromley RG, Miller J (1996) Plio-Pleistocene sedimentation in oscillating grabens north-east Rhodes, Greece. Geol J 31:271–296

Hansen KS (1999) Development of a prograding carbonate wedge during sea level fall: Lower Pleistocene of Rhodes, Greece. Sedimentology 46:599–576. https://doi.org/10.1046/j.1365-3091.1999.00238.x

Heldal T, Meyer GB, Dahl R (2015) Global stone heritage Larvikite Norway. Geol Soc Special Publicat. https://doi.org/10.1144/SP407.14

Hernández-Montes E, Gil-Martín LM, Coletti C, Dilaria S, Germinario L, Mazzoli C (2022) Prediction model for the evolution of the deterioration of bricks in heritage buildings in venice caused by climate change. Heritage 6:483–491. https://doi.org/10.3390/heritage6010025

Horai KI (1971) Thermal conductivity of rock-forming minerals. J Geophys Res 76(5):1278–1308. https://doi.org/10.1029/JB076i005p01278

Jalón ML, Chiachío J, Gil-Martín LM, Hernández-Montes E (2020) Probabilistic identification of surface recession patterns in heritage buildings based on digital photogrammetry. J Build Eng. https://doi.org/10.1016/j.jobe.2020.101922

EN ISO 12571 (2000) *Hygrothermal performance of building materials and products - Determination of hygroscopic sorption properties*. CEN, Brussels

EN ISO 12572 (2001) *Hygrothermal performance of building materials and products - Determination of water vapour transmission properties*. CEN, Brussels

Klopfer H (1985) Feuchte. In: Lutz P, Jenisch R, Klopfer H, Freymuth H, Krampf L (eds) Lehrbuch der Bauphysik: Schall, Wärme, Feuchte, Licht, Brand. Teil 1 einer Baukonstruktionslehre. B. G. Teubner: Stuttgart, pp 265–434.

Kollias EE (1989) The building materials of the monuments of the medieval city of Rhodes and the compatibility problems with maintenance. In: Compatible materials for the protection of European cultural heritage, Pact 56, Incomarech - Raphael 97/E/412, pp 247–257.

Kontozova-Deutscha V, Cardell C, Urosevic M, Ruiz Agudo E, Deutsch F, Van Grieken R (2011) Characterization of indoor and outdoor atmospheric pollutants impacting architectural monuments: the case of San Jerónimo Monastery (Granada, Spain). Environ Earth Sci 63:1433–1445. https://doi.org/10.1007/s12665-010-0657-5

Kušnerová M, Valíček J, Harničárová M, Hryniewicz T, Rokosz K, Palková Z, Václavík V, Řepka M, Bendová M (2013) A proposal for simplifying the method of evaluation of uncertainties in measurement results. Measure Sci Rev 13(1):1–6. https://doi.org/10.2478/msr-2013-0007

Lazzarini L, Antonelli F, Cancelliere S, Conventi A (2008) The deterioration of Euganean Trachyte in Venice. In: Proceedings of the 11th International Congress on Deterioration and Conservation of Stone, 15–20 September, Torun, 110, pp 153–163.

Lazzarini L (2012) Pietra d'Istria: quarries, characterization, deterioration of the stone of Venice. 12th International Congress on the Deterioration and Conservation of Stone, 22–26 October, Columbia University, New York.

Lekkas E, Danamos G, Skourtsos E (2007) Implications for the correlation of the hellenic nappes in sw aegean: the geological structure of the archangelos region, rhodes Island. Bulletin Geol Soc Greece 40:374–385. https://doi.org/10.12681/bgsg.16622

Lionello P, Barriopedro D, Ferrarin C, Nicholls RJ, Orlić M, Raicich F, Reale M, Umgiesser G, Vousdoukas M, Zanchettin D (2021) Extreme floods of Venice: characteristics, dynamics, past and future evolution (review article). Nat Hazard 21:2705–2731. https://doi.org/10.5194/nhess-21-2705-2021

López-Quirós A, Barbier M, Martín JM, Puga-Bernabéu Á, Guichet X (2016) Diagenetic evolution of Tortonian temperate carbonates close to evaporites in the Granada Basin (SE Spain). Sed Geol 335:180–196. https://doi.org/10.1016/j.sedgeo.2016.02.011

Luque A, Cultrone G, Mosch S, Siegesmund S, Sebastian E, Leiss B (2010) Anisotropic behaviour of white macael marble used in the alhambra of granada (Spain). The role of thermohydric expansion in stone durability. Eng Geol 115(3–4):209–216. https://doi.org/10.1016/j.enggeo.2009.06.015

Le Maitre RW, Streckeisen A, Zanettin B, Bas MJL, Bonin B, Bateman P (2005) Igneous Rocks: A classification and glossary of terms: recommendations of the International Union of Geological Sciences Subcommission on the Systematics of Igneous Rocks. In: Le Maitre RW (ed) Cambridge University Press. https://doi.org/10.1007/s13398-014-0173-7.2

Maniatis Y, Tambakopoulos D, Dotsika E, Wescoat BD, Matsas D (2012) The sanctuary of the Great Gods-Samothrace, an extended marble provenance study. In: Gutiérrez Garcia A, Lapuente P, Rodà I (eds) Interdisciplinary Studies on Ancient Stone: Proceedings of the IXth International Conference of the Association for the Study of Marbles and Other Stones in Antiquity (ASMOSIA). Tarragona, Spain, pp 263–278

Maniatis Y, Tambakopoulos D, Papavassiliou E, Bairami K (2015) Lartios Lithos of Rhodes Island: scientific characterization and possible uses and exports. Split, Croatia, pp 18–22

Maritan L, Mazzoli C, Sassi R, Speranza F, Zanco A, Zanovello P (2013) Trachyte from the Roman aqueducts of Padua and Este (north-east Italy): A provenance study based on petrography, chemistry and magnetic susceptibility. Eur J Mineral 25:415–427. https://doi.org/10.1127/0935-1221/2013/0025-2282

Masetti D, Figus B, Jenkyns HC, Barattolo F, Mattioli E, Posenato R (2017) Carbon-isotope anomalies and demise of carbonate platforms in the Sinemurian (Early Jurassic) of the Tethyan region: evidence from the Southern Alps (Northern Italy). Geol Mag 154:625–650. https://doi.org/10.1017/S0016756816000273

Milizia E, Brandano M, Cornale P, Mazzoli C, Perissinotto ML, Preto N, Tomassetti L (2022) Vicenza stone: nomination as global heritage stone resource. Italy, Torino, pp 19–21

Molina E, Cultrone G, Sebastian E, Alonso FJ, Carrizo L, Gisbert J, Buj O (2011) The pore system of sedimentary rocks as a key factor in the durability of building materials. Eng Geol 118:110–121. https://doi.org/10.1016/j.enggeo.2011.01.008

Molina E, Cultrone G, Sebastian E, Alonso FJ (2013) Evaluation of stone durability using a combination of ultrasound, mechanical and accelerated aging tests. J Geophys Eng 10:035003. https://doi.org/10.1088/1742-2132/10/3/035003

Molina E, Arizzi A, Benavente D, Cultrone G (2020) Influence of surface finishes and a calcium phosphate-based consolidant on the decay of sedimentary building stones due to acid attack. Front Mater 7:581979. https://doi.org/10.3389/fmats.2020.581979

Molli G, Giorgetti G, Meccheri M (2000) Structural and petrological constrains on the tectono-metamorphic evolution of the Massa Unit (Alpi Apuane, NW Tuscany, Italy). Geol J 35:251–264. https://doi.org/10.1002/gj.860

Moropoulou A, Koui M, Theoulakis P, Bakolas A, Roumpopoulos K, Michailidis P, Van Grieken R, Cardell-Fernandez C (2000) Microstructural criteria for the evaluation of stone susceptibility to sea-salt decay. In: Galàn E, Zezza F (eds) Protection and conservation of the cultural heritage of the Mediterranean cities Proceedings of the 5th International Symposium on the conservation of monuments in the Mediterranean basin. Sevilla, Spain, pp 5–8

Mutti E, Orombelli G, Pozzi R (1970) Geological studies on the Dodecanese islands (Aegean Sea). 9. Geological map of the island of Rhodes (Greece). Explanatory notes. Ann Géol Pays Hellén 22:77–226

Navarro R, Pereira D, Cruz AS, Carrillo G (2019) The Significance of "White Macael" marble since ancient times: characteristics of a candidate as Global Heritage Stone Resource. Geoheritage 11:113–123. https://doi.org/10.1007/s12371-017-0264-x

Navarro R, Molina E, Baltuille JM (2013) The relevance of 'Santa Pudia' Calcarenite: a natural stone to preserve heritage buildings in Andalusia (Spain). Geophysical Research.

Nebelsick JH, Rasser MW, Bassi D (2005) Facies dynamics in Eocene to Oligocene circumalpine carbonates. Facies 51:197–217. https://doi.org/10.1007/s10347-005-0069-2

Nebelsick JH, Bassi D, Lempp J (2013) Tracking paleoenvironmental changes in coralline algal-dominated carbonates of the Lower Oligocene Calcareniti di Castelgomberto Formation (Monti Berici, Italy). Facies 59(1):133–148. https://doi.org/10.1007/s10347-012-0349-6

Neumann E-R, Wilson M, Heeremans M, Spencer EA, Obst K, Timmerman MJ, Kirstein L (2004) Carboniferous-Permian rifting and magmatism in southern Scandinavia, the North Sea and northern Germany: a review. Geol Soc London Special Publicat. https://doi.org/10.1144/GSL.SP.2004.223.01.02

Papavassiliou E, Bairami K, Maniatis Y, Tambakopoulos D (2020) The usage of Lartian stone through the centuries. In: Panagiotaki M, Tomazos I, Papadimitrakopoulos F (eds) Cutting-edge Technologies in Ancient Greece: Materials Science applied to trace ancient technologies in the Aegean world. Oxbow Books, NY, pp 165–172

Pimienta L, Klitzsch N, Clauser C (2018) Comparison of thermal and elastic properties of sandstones: Experiments and theoretical insights. Geothermics 76:60–73. https://doi.org/10.1016/j.geothermics.2018.06.005

Piovesan R, Tesser E, Maritan L, Zaccariello G, Mazzoli C, Antonelli F (2023a) Mapping of stones and their deterioration forms: the Clock Tower, Venice (Italy). Heritage Science 11:108. https://doi.org/10.1186/s40494-023-00909-4

Piovesan R, Mazzoli C, Maritan L (2023b) Production recipes of mortar-based materials from ancient Pompeii by quantitative image analysis approach: the microstratigraphy of plasters in the Temple of Venus. J Cult Herit 59:57–68. https://doi.org/10.1016/j.culher.2022.11.002

Piovesan R, Tesser E, Bruschi G, Faccio P, Antonelli F (2024) Giuseppe Torres's "Byzantine house" in Venice: building materials and deterioration products of an early 1900s home in the lagoon environment. Stud Conserv 69(8):690–706. https://doi.org/10.2139/ssrn.4396978

Platt JP, Anczkiewicz R, Soto J-I, Kelley SP, Thirlwall M (2006) Early Miocene continental subduction and rapid exhumation in the western Mediterranean. Geology 34(11):981–984. https://doi.org/10.1130/G22801A.1

Préat A, Morano S, Loreau J-P, Durlet C, Mamet B (2006) Petrography and biosedimentology of the Rosso Ammonitico Veronese (middle-upper Jurassic, north-eastern Italy). Facies 52:265–278. https://doi.org/10.1007/s10347-005-0032-2

Primavori P (2015) Carrara Marble: a nomination for 'Global Heritage Stone Resource' from Italy. In: Pereira D, Marker BR, Kramar S, Cooper BJ, Schouenborg BE (eds), Global Heritage Stone: Towards International Recognition of Building and Ornamental Stones. Geological Society, London, Special Publications 407, 137–154. https://doi.org/10.1144/SP407.21

Primavori P (2020) Rosso Verona marble (Italy): proposed as a candidate for "Global Heritage Stone Resource". EGU General Assembly 2020, Online, 4-8 May 2020, EGU2020-2873. https://doi.org/10.5194/egusphere-egu2020-2873

Renzulli A, Antonelli F, Santi P, Busdraghi P, Luni M (1999) Provenance determination of lava flagstones from the Roman "via Consolare Flaminia" pavement (Central Italy) using petrological investigations. Archaeometry 41(2):209–226. https://doi.org/10.1111/j.1475-4754.1999.tb00978.x

Rodriguez-Navarro C, Sebastian E (1996) Role of particulate matter from vehicle exhaust on porous building stones (limestone) sulfation. Sci Total Environ 187:79–91. https://doi.org/10.1016/0048-9697(96)05124-8

Rodriguez-Navarro C (1994) Causas y mecanismos de alteración de los materiales calcáreos de las Catedrales de Granada y Jaén. PhD Thesis. University of Granada.

Ruedrich J, Bartelsen T, Dohrmann R, Siegesmund S (2011) Moisture expansion as a deterioration factor for sandstone used in buildings. Environ Earth Sci 63:1545–1564. https://doi.org/10.1007/s12665-010-0767-0

Ruiz-Agudo E, Lubelli B, Sawdy A, van Hees R, Price C, Rodriguez-Navarro C (2011) An integrated methodology for salt damage assessment and remediation: the case of San Jerónimo Monastery (Granada, Spain). Environ Earth Sci 63:1475–1486. https://doi.org/10.1007/s12665-010-0661-9

Ruiz-Agudo E, Ibañez-Velasco A, Ruiz-Agudo C, Bonilla-Correa S, Elert K, Rodríguez-Navarro C (2024) Damage of porous building stone by sodium carbonate crystallization and the effect of crystallization modifiers. Constr Build Mater 411:134591. https://doi.org/10.1016/j.conbuildmat.2023.134591

Salvi AM, Langerame F, Macchia A, Sammartino AP, Tabasso ML (2012) XPS characterization of (Copper-based) coloured stains formed on limestone surfaces of outdoor Roman monuments. Chem Central J. https://doi.org/10.1186/1752-153X-6-S2-S10

Salvini S, Bertoncello R, Coletti C, Germinario L, Maritan L, Massironi M, Pozzobon R, Mazzoli C (2022) Recession rate of carbonate rocks used in cultural heritage: Textural control assessed by accelerated ageing tests. J Cult Herit 57:154–164. https://doi.org/10.1016/j.culher.2022.08.010

Salvini S, Coletti C, Maritan L, Massironi M, Pieropan A, Spiess R, Mazzoli C (2023a) Petrographic characterization and durability of carbonate stones used in UNESCO World Heritage Sites in Northeastern Italy. Environ Earth Sci 82(1):49. https://doi.org/10.1007/s12665-022-10732-y

Salvini S, Coletti C, Maritan L, Massironi M, Balsamo F, Mazzoli C (2023b) Exploring the pore system of carbonate rocks through a multi-analytical approach. Environ Earth Sci 82:564. https://doi.org/10.1007/s12665-023-11234-1

Schirolli P (1997) La successione liassica nelle Prealpi Bresciane centro-occidentali (Alpi Meridionali, Italia): stratigrafia, evoluzione paleogeografico-strutturale ed eventi connessi al rifting. Atti Ticinensi di Scienze della Terra. Serie Speciale 6:5–137

Schirolli P (2007) Studio macroscopico dei materiali lapidei locali impegnati nelle epigrafi bresciane di età Alto-Medievale. Natura Bresciana 35:13–33

Schou-Jensen E, Neumann E-R (1988) Volcanic rocks on Jeløya, central Oslo Region: the mafic lavas. Nor Geol Tidsskr 68:289–308

Sciarretta F, Antonelli F, Peron F, Caniglia S (2018) Final outcomes on the multi-disciplinary long-term monitoring and preservation state investigation on the medieval external Façades of Palazzo Ducale in Venice, Italy. J Civ Struct Heal Monit 8(1):111–133. https://doi.org/10.1007/s13349-017-0263-2

Shabani A, Feyzabadi M, Kioumarsi M (2022) Model updating of a masonry tower based on operational modal analysis: The role of soil-structure interaction. Case Stud Construct Mater 16:e00957. https://doi.org/10.1016/j.cscm.2022.e00957

Stamati Z, Stefanakis MI, Kontogianni G, Georgopoulos A (2022) Virtual reconstruction of the temple on the Acropolis of Kymissala in Rhodes. Digital 2(2):296–319. https://doi.org/10.3390/digital2020017

Stefanis N-A, Theoulakis P, Pilinis C (2009) Dry deposition effect of marine aerosol to the building stone of the medieval city of Rhodes, Greece. Build Environ 44:260–270. https://doi.org/10.1016/j.buildenv.2008.03.001

Taelman D, Delpino C, Antonelli F (2019) Marble decoration of the Roman Theatre of Urvinum Mataurense (Urbino, Marche Region, Italy): an archaeological and archaeometric multimethod provenance study. J Cult Herit 39:238–250. https://doi.org/10.1016/J.CULHER.2019.03.009

Tesser E, Antonelli F (2018) Evaluation of silicone based products used in the past as today for the consolidation of Venetian monumental stone surfaces. Mediter Archaeol Archaeom 18(5):159–170. https://doi.org/10.5281/zenodo.1285902

Tesser E, Antonelli F, Sperni L, Ganzerla R, Maravelaki N-P (2014) Study of the stability of siloxane stone strengthening agents. Polym Degrad Stab 110:232–240. https://doi.org/10.1016/j.polymdegradstab.2014.08.022

Tesser E, Lazzarini L, Ganzerla R, Antonelli F (2017) The decay of the polysiloxane resin Sogesil XR893 applied in the past century for consolidating monumental marble surfaces. J Cult Herit 27:107–115. https://doi.org/10.1016/j.culher.2017.11.002

Tesser E, Lazzarini L, Bracci S (2018) Investigation on the chemical structure and ageing transformations of the cycloaliphatic epoxy resin EP2101 used as stone consolidant. J Cult Herit 31:72–82. https://doi.org/10.1016/j.culher.2017.03.001

Titschack J, Bromley RG, Freiwald A (2005) Plio-Pleistocene cliff-bound, wedge-shaped, warm-temperate carbonate deposits

from Rhodes (Greece): Sedimentology and facies. Sed Geol 180:29–56. https://doi.org/10.1016/j.sedgeo.2005.06.009

Vázquez P, Alonso FJ, Carrizo L, Molina E, Cultrone G, Blanco M, Zamora I (2013) Evaluation of the petrophysical properties of sedimentary building stones in order to establish quality criteria. Constr Build Mater 41:868–878. https://doi.org/10.1016/j.conbuildmat.2012.12.026

Warr LN (2021) IMA-CNMNC approved mineral symbols. Mineral Mag 85(3):291–320. https://doi.org/10.1180/mgm.2021.43

Zaccariello G, Tesser E, Piovesan R, Antonelli F (2024) The (building) stones of Venice under threat: a study about their deterioration between climate change and land subsidence. Sustainability 16(11):4701. https://doi.org/10.3390/su16114701

Zuffa G (1980) Hybrid arenites: their composition and classification. J Sediment Res. https://doi.org/10.1306/212F7950-2B24-11D7-8648000102C1865D